공학박사 학위논문

Hydrodynamic analysis of the optimal design of fish gills and human lung

물고기 아가미와 인간 폐의 최적 설계에 대한

유체역학적 고찰

2015년 2월

서울대학교 대학원

기계항공공학부

박 근 환

Hydrodynamic analysis of the optimal design of fish gills and human lung

물고기 아가미와 인간 폐의 최적 설계에 대한 유체역학적 고찰

지도 교수 김 호 영

이 논문을 공학박사 학위논문으로 제출함

2015 년 2월

서울대학교 대학원
기계항공공학부
박 근 환

박근환의 박사 학위논문을 인준함

2015 년 2 월

위 원 장 _____ (인)

부위원장 _____ (인)

위 원 _____ (인)

위 원 _____ (인)

위 원 _____ (인)

Abstract

Hydrodynamic analysis of the optimal design of fish gills and human lung

Keunhwan Park
Department of Mechanical and Aerospace Engineering
The Graduate School
Seoul National University

It is generally assumed that shapes encountered in nature have evolved in a way as to maximize the robustness of a species. Nevertheless, given natures notoriously complex designs, it is often unclear what is being optimized. We here consider the optimization design principle in two respiratory systems: fish gills and human lung.

The lamellar pattern of fish gills is one of the few cases in which optimization in nature can be well defined. We demonstrate that the lamellar pattern of fish gills has been optimized, such that fish display interlamellar spaces of similar dimension regardless of body mass or species. It is suggested that the primary evolutionary pressure on fish gills is to maximize the oxygen transfer rate under given pressure drop. This natural optimization strategy demonstrates how control of the channel arrangement in microfluidic devices enhances heat and mass transfer.

Lungs are natural microfluidic networks that transport oxygen from air into blood stream. The diameter reduction ratio of airways of lung determines the efficiency of physiological processes. An optimal diameter reduction ratio is thus expected. We here develop a mathematical model for diffusion transport of acinar airway and unveil the origin of the observed diameter reduction ratio of acinar airways. The energy cost of acinar

airways is shown to be minimized for a given amount of oxygen transport, suggesting modified Murrays law for acinar airways.

Keywords : fish respiration, human respiration, oxygen transfer, biofluiddynamics
Student Number : 2008-20743

Contents

List of Figures

Chapter 1

Introduction

Animals are believed to be living mass transfer systems, being involved in the constant exchange of mass with their external environment. Actions such as feeding and drinking, which can be described as the transfer of mass from the external environment to the body, are important in order to provide nutrients and water to animal cells (1, 2). Mass transfer occurs from each cell to the entire body; this action facilitates important roles, such as communications between the internal and external environments of a cell and between cells (3), protein production and tissue construction and delivery of nerves signals to the brain and other body parts (4).

Respiration is an important mass transfer activity performed by animals, where oxygen is transferred from the surrounding environment to the cells and carbon dioxide from the cells to the environment (5). When oxygen is delivered to the cells within tissues, cellular respiration occurs which refers the metabolic process by which an organism obtains energy by reacting oxygen with glucose to give water, carbon dioxide and adenosine triphosphate cycle (ATP). Unlike other mass transfer activities performed by animals, such as feeding and drinking, respiration is a constant process and cannot be discontinued, even for a short period of time, as the lack of oxygen would immediately result in cell death. Therefore, exchange of oxygen and carbon dioxide occurs in animals at all times, even during sleep.

Respiratory gas exchange primarily occurs via diffusion. Diffusion is a transport mechanism driven by a concentration gradient, where a substance moves from a high concentration region to a region of low concentration. Ficks law provides the universal equation governing diffusion: $Q = DA\nabla\phi$, where Q denotes the gas transfer rate, D is the diffusion coefficient for gas transport in respiratory fluids, A is the cross-sectional area of the respira-

tory system that is in contact with the respiratory fluids and ϕ is the gas concentration in the respiratory fluids. Accordingly, the oxygen transfer rate is maximized when the distance between the respiratory fluids and blood is low and the cross-sectional area of the respiratory system is large. Although the exchange of gas via diffusion does not necessitate energy consumption, the supply of fresh respiratory fluids to the region where oxygen transfer occurs requires a lot of energy. Consequently, efficient respiration necessitates minimizing the energy cost of supplying fresh respiratory fluids to the respiratory system. In addition, the respiratory systems must comprise a large surface area and thin membrane structures, in order to maximize oxygen transfer with the fresh respiratory fluid.

However, the largest surface area with thin membrane and the smallest energy cost of supplying the fresh air cannot be suitable for respiratory systems because external environments are not amicable to respiration. The first reason is that when the respiration fluids are air, the relatively low humidity of air compared to blood causes desiccation of respiratory systems through diffusion of water from blood to air(6-8). Similar problems are observed even when water is the respiratory fluid. Water has a low concentration of oxygen and displays low diffusivity of oxygen; on the other hand, the density and viscosity of water is greater than that of air. Therefore, aquatic creatures require a greater amount of energy to supply water to the respiratory system, which is characterized by dense membrane structures for extended surface area (9-14). When the fluid is brine, the respiratory system should work additionally, as the difference in osmotic pressures between water and blood could cause critical damage to the animal tissues (15-19). Another major reason causing the improper functioning of the system is that a large, extended surface area of the thin-membrane respiratory system is vulnerable to attack from parasites and infection from the external environment (20, 21). Temperature differences between the respiratory systems and the respiratory fluids is another problem, which leads to rapid heat loss in the body parts via the thin membranes of the respiratory systems (22, 23). Therefore, the design of animal respiratory systems have evolved to overcome these problems over tens of billions of years.

Interestingly, the respiratory system is designed differently in each animal, as shown in Figure 1.1. This may be a result of the differences in the living conditions and environment or the medium of oxygen consumption for each animal. The latter is based on the oxygen consumption rate of animals. According to Kleibers law, the rate of oxygen consumption increases in proportion to the three-fourth power of the body mass, as shown in Fig-

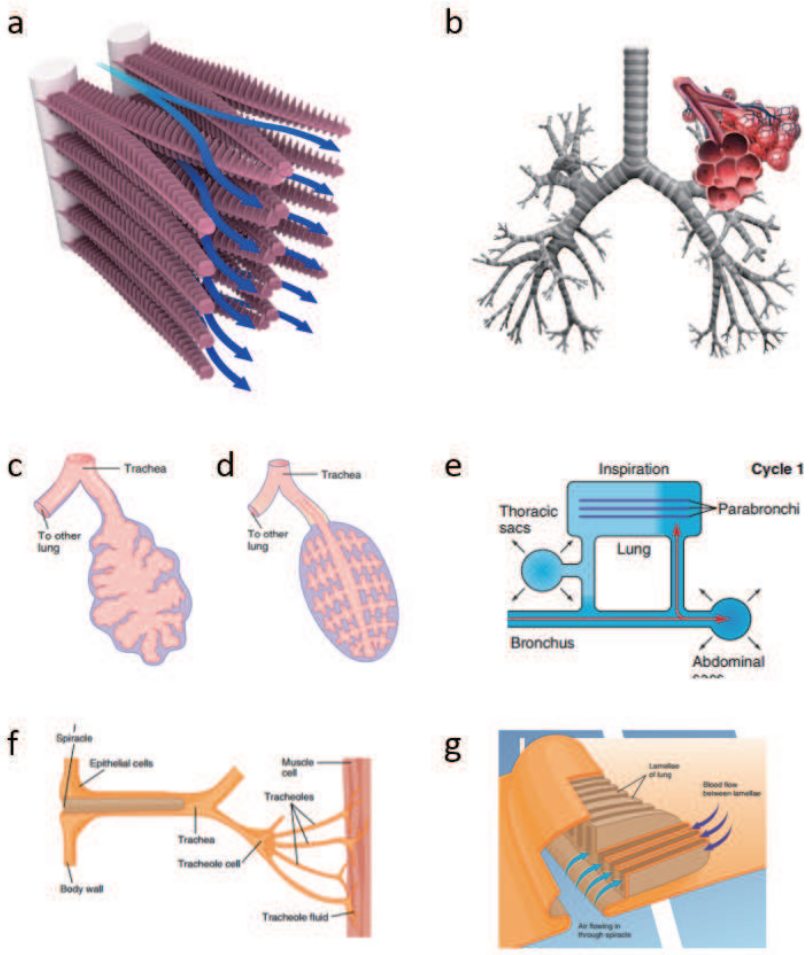

Figure 1.1: Schematic illustration of the respiratory systems of various animals. The respiratory system of each animal is made up of a different design. Illustrated here are the (a) gills of fish, (b) lungs of mammals, (c) amphibians, (d) reptiles, (e) and avian species. (f) The tracheal system of an insect and (g) book lungs of spiders are also pictured. Images (c), (d), (e), (f) and (g) were taken from SA Miller *et al.*(2002).

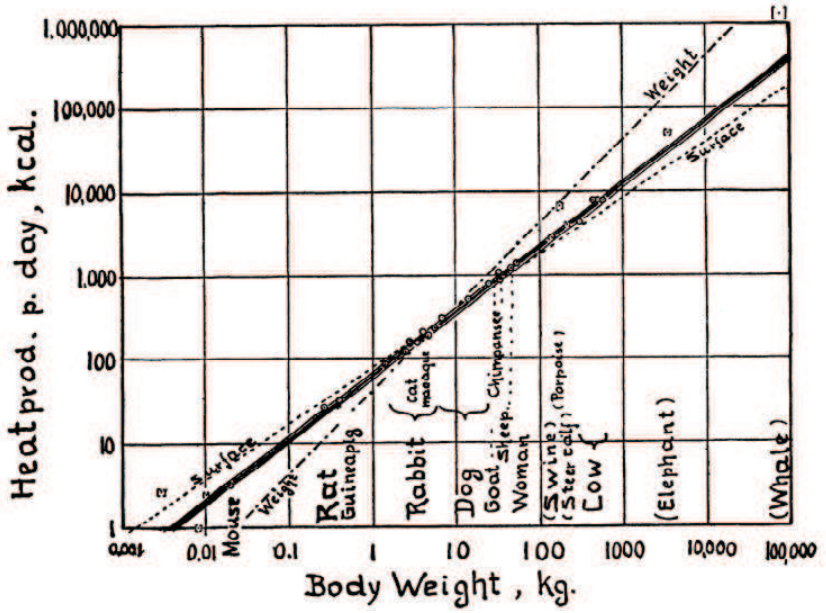

Figure 1.2: Body size versus the metabolic rate of a variety of species of animals. The metabolic rate of many species follows the three-fourth power law of body mass. This is known as the Kleibers law. Originally published in Kleiber (1947).

ure 1.2 (25-27). On the other hand, the amount of oxygen transported is proportional to the surface area of the respiratory system, which is scaled up to the one-third power of body mass (26, 27). Therefore, the respiratory system of animals differs according to the body size of the animals, in order to afford the rapid increase in the rate of oxygen consumption.

Despite this, we believe that the evolution of the respiratory system accommodates efficient oxygen transport, in addition to adaptation to the tough surrounding environment and changes in body size in order to supply the oxygen demand of each species, as a good respiratory efficiency is critically important to maximize the robustness of the species. For hundreds of years, biologists have devoted a great deal of effort towards elucidating the method by which the respiratory systems conduct all physical functions in animals (9, 24). However, very few researchers investigated the optimization of the respiratory system. This is because the respiratory system is sufficiently complex and the function that is being optimized, as well as its relevant constraints, remain unclear.

In this thesis, we have focused on the design principles of fish gills and human lungs; these were investigated as the gills of fish are part of a respiratory system that extracts dissolved oxygen from water and study of the design principle of human lungs is valuable in order to understand and elucidate respiratory illnesses, such as asthma, influenza and bronchitis. In this thesis, we have considered the fluid mechanics of the natural respiratory strategies of fish gills and human lungs, with a view towards defining the optimal transport strategies.

1.1 Optimal lamellar arrangement in fish gills

In chapter 2, we consider the design of fish gills. Gills have evolved exclusively in aquatic creatures to extract oxygen under water. It consist of thread-like structures called filaments which are covered by an array of lamellae enclosing a capillary blood network. Oxygen-rich water passes through the narrow channels formed by the lamellar layers, where oxygen diffuses into the capillaries. The densely packed lamellar structure is advantageous because it provides a large surface area for oxygen transfer, but it also generates severe viscous resistance. Accordingly, because interlamellar distance determines both the surface area for oxygen diffusion and the size of the water flow channel, we can expect an optimal interlamellar distance for maximizing the oxygen transfer at a given pumping pressures.

We have collected 75 species fish gill data including filament length, lamellar length, lamellar height and interlamellar distance. Remarkably,

although the body mass of our fish gill data varies from 0.1 g to 100 kg, the interlamellar distance typically remains on the order of 40 μm.

In order to rationalize the observed interlamellar distance in the gills of various fish species, we have developed a mathematical model depicting oxygen transportation via interlamellar water flow. We assumed the water flow in the interlamellar channel to be a two dimensional channel flow, as the height of the lamella is much greater than the interlamellar distance. Based on this assumption, the lamellar channel oxygen transfer rate was obtained by taking into account the mass and momentum conservation of oxygen and water comprising the lamellar channel flow, respectively. Based on the anatomical observations, the oxygen transfer rate of the lamellar channel water flow was further assumed to be a function of interlamellar distance. As a result, an optimal interlamellar distance required to maximize the oxygen transfer rate may be obtained.

Engineered fish gills were fabricated to validate the developed mathematical model of oxygen transfer. An oxygen-rich water channel was sandwiched between two neighbor counter flow channels of oxygen-depleted water. The oxygen partial pressure was measured at the outlet of the oxygen-rich water channel for various channel dimensions. Thereby, our mathematical model was found to be consistent with the experimental results.

Chapter 2 appears as published in Park, K., Kim, W., & Kim, H. Y. (2014). Optimal lamellar arrangement in fish gills. Proceedings of the National Academy of Sciences, 111(22), 8067-8070.

1.2 Physical principle of acinar airway design in human lungs

Lungs are natural microfluidic devices that transport oxygen from air to the blood stream. The airways show a hierarchy of branchial trees. The trachea is divided into bronchi, which is divided into bronchioles. This process of subdivision is continued down to the terminal bronchioles which are the smallest airways expressing no alveoli. The bronchi are also called conducting airways. The terminal bronchioles are divided into respiratory bronchioles, called acinar airways. These are divided into the alveolar ducts, which are completely covered with alveoli. Oxygen diffuses out of the alveoli, across the alveolar epithelium and the capillary endothelium, into hemoglobin in the blood. The large number of alveoli provides a large surface area to facilitate oxygen exchange. Airways are branched by dichotomy, with a systematic reduction in size. The duct diameter varies

over 3 orders of magnitude, from 10 cm to 0.1 mm. The observed diameter reduction ratio of the conducting airways is known as the Hess-Murray law and is closely related to the minimization of viscous dissipation. However, the diameter reduction in the acinar airways is more moderate compared to the conducting airways and is therefore larger than the predicted value from the Hess-Murray law.

In this study, we have described the design principle of diameter reduction ratio in the acinar airways. The dominant transfer mechanism in acinar airways is diffusion, unlike the conducting airways. Therefore, we have constructed a mathematical model for oxygen transfer through a series of acinar airways. Our model allows the prediction of the optimal diameter reduction ratio in acinar airways that minimizes the energy cost of acinar airways, thereby rationalizing the observed airway reduction ratio in the acinar airways.

Chapter 2

Optimal lamellar arrangement in fish gills

2.1 Introduction

Fish gills have evolved exclusively in aquatic creatures to extract aqueous oxygen. Because oxygen has considerably low solubility and diffusivity in water, the efficiency of respiration is critical (28). Gills consist of plate-like structures called filaments that are covered by an array of lamellae enclosing a capillary blood network, as shown in Figure 2.1, and Figure 2.2 (28, 29). Oxygen-rich water passes through the narrow channels formed by the lamellar layers, where oxygen diffuses into the capillaries. The densely packed lamellar structure is advantageous because it provides a large surface area for oxygen transfer; however, it also generates considerable viscous resistance. This resistance is overcome by pumping. Fish typically adopt one of the following two pumping mechanisms: branchial pumping and ram ventilation. Most teleost fish, members of the diverse group of ray-finned fish, employ branchial pumping, and muscular compression in the pharynx enables water flow through the gills. In ram ventilation, which is used by many pelagic fish, the dynamic pressure generated by their swimming drives water flow into the gills (30).

Most previous studies on the structure of fish gills have focused on the dependence of the total surface area of the gill upon the body size and species of fish (28, 31, 32). We consider the convective oxygen transfer that occurs in fish gills. As water passes through the narrow lamellar channels, increased viscous resistance impedes water flow at a given pumping pressure, which is limited by muscle power or swimming speeds. This leads to

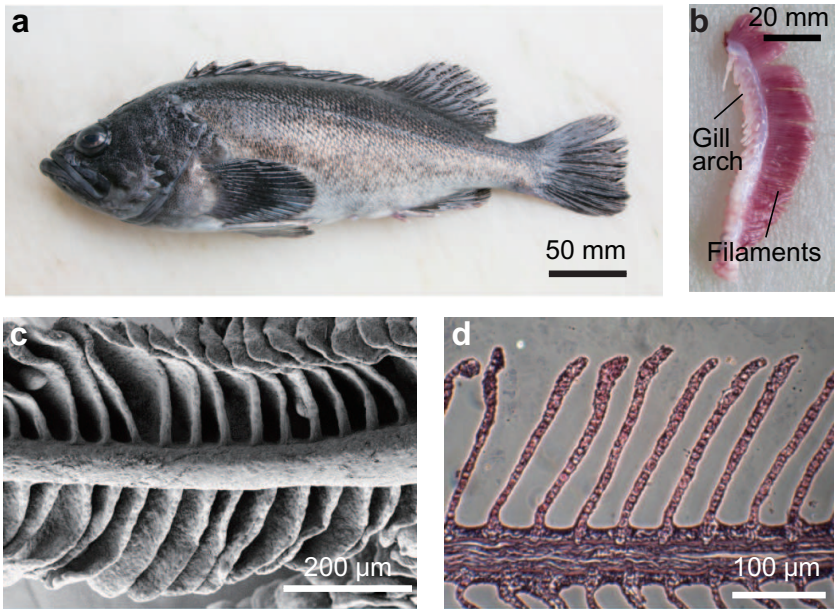

Figure 2.1: The branchial apparatus of a rockfish Sebastes schlegelii. (*a*) Sebastes schlegelii having gills on both sides of the pharynx. (*b*) The gill arch and filaments. (*c*) Scanning electron microscopy (SEM) image of a gill filament. (*d*) Hematoxylin and eosin (H&E)-stained cross-section of a gill filament.

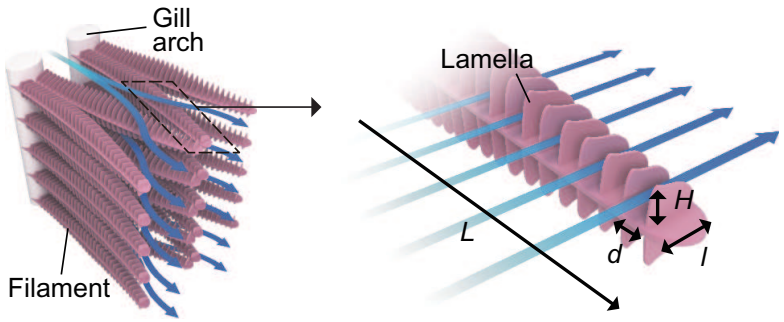

Figure 2.2: A schematic illustration of gill morphology. Plate-like filaments hanging on branchial arches are covered with lamellae enclosing a blood capillary network. The blue arrows indicate the direction of water flow from the gill arches to the operculum. The well-ordered lamellar structures provide arrays of microchannels where oxygen diffuses to the capillaries.

a lowering of the oxygen transfer rate. Hence, the flow rate within the gaps of the lamellae and the extended surface area play important roles in determining the oxygen transfer rate. The number of lamellae per unit length of gill filament determines both the surface area for diffusion and the size of the water channels. Therefore, we investigate the relationship between lamellar distance and oxygen transfer rate, an aspect that previously has seldom been explored.

2.2 Theoretical analysis

We compiled interlamellar distances in a broad range of fish species, as shown in Figure 2.3. It is remarkable that whereas the body mass of these species varies over six orders of magnitude from 0.1 g to 100 kg, the interlamellar distances vary within a very small range, approximately 20 to 100 μm (33, 34). To explain the relatively uniform interlamellar distances, we mathematically modeled the oxygen transfer rate in fish gills, which is driven by the gradient of oxygen partial pressure. For an infinitesimal control volume shown in Figure 2.4, the conservation of oxygen can be written as $dQ_o/dx = -h\beta s(P_w - P_b)$, where Q_o is the oxygen flow rate, h the convective mass transfer coefficient, β the oxygen solubility coefficient of water, s the wetted perimeter of the control volume, P_w the average oxygen partial pressure in water, and P_b the oxygen partial pressure on the lamellar surface. The oxygen flow rate can be expressed in terms of the water flow rate through the channel Q_w as $Q_o = Q_w\beta P_w$. Because the lamellar height $H \sim 400$ μm is typically much greater than the interlamellar distance $d \sim 40$ μm, as shown in Figure 2.3 (29, 35-38), $s \sim 2H$, which allows us to write

$$Q_w \frac{dP_w}{dx} + 2hH(P_w - P_b) = 0 \tag{2.1}$$

For the characteristic flow speed through interlamellar channels $u \sim 0.01$ m/s (29, 38), water density $\rho \sim 1000$ kg/m^3, viscosity $\mu \sim 0.001$ Pa $\cdot$ s, interlamellar distance $d \sim 10$ μm, and lamellar length $l \sim 1$ mm, the ratio of inertial to viscous effects, prescribed by the Reynolds number $\mathrm{Re} = \rho u d^2/\mu l \sim 10^{-3}$, implies that the flow within the interlamellar channel is laminar with negligible entrance effects. Accordingly, h is given by $h = \mathrm{Sh}D_w/(2d)$, where Sh is the Sherwood number, the ratio of convective to diffusive mass transfer (39), which is estimated as 7.5, and D_w, the oxygen diffusion coefficient in water (40), is 2×10^{-9} m^2/s.

To solve Eq. 2.1 for P_w as a function of x, we first consider the x dependency of P_b. One expects that P_b approximates the partial pressure

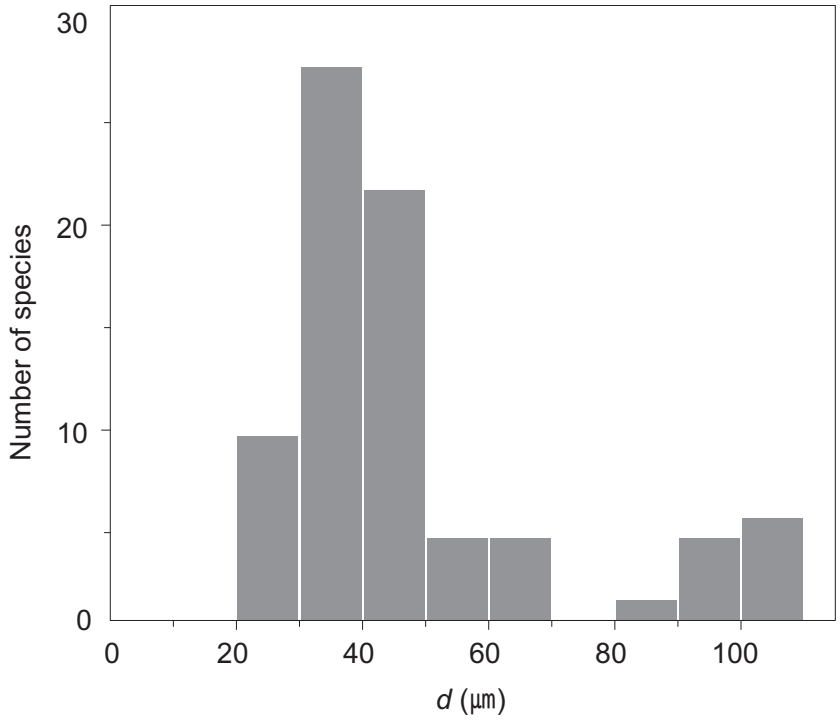

Figure 2.3: Distribution of interlamellar distances for 75 fish species. The gill interlamellar distances of most fish species range from 20 to 110 μm despite immense variation in their body masses, from 10^{-1} to 10^{5} g. We assumed that the lamellar thickness is negligible compared to the interlamellar distance, and estimated the interlamellar distance d as a reciprocal of the number of lamellae per unit length of the gill filament (29, 32). Detailed data and their sources are provided in Table A.1

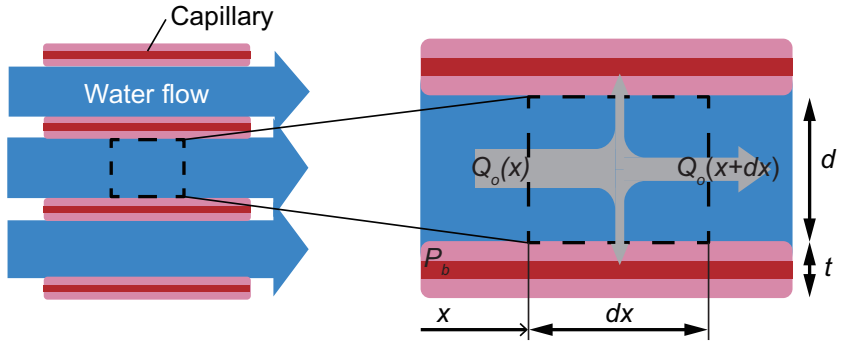

Figure 2.4: A schematic illustration of the top view of the interlamellar channels. The dashed box corresponds to the control volume for the mass-transfer analysis.

of oxygen in the capillaries due to negligible diffusive resistance between the lamellar surface and the capillaries. Hemoglobin in the capillaries rapidly combines with oxygen molecules, thus stabilizing the partial pressure of oxygen at a relatively low value (41-44). Hence, the relative variation in partial pressure in capillaries to that in water $\Delta P_b/\Delta P_w \ll 1$, allowing us to neglect the variation of P_b with x. Solving Eq. 2.1 yields $P_w(x) = (P_{wo}-P_b)\exp(-2bHx/Q_w)+P_b$, where P_{wo} is the partial pressure of oxygen at the entrance $x = 0$. Since the rate of oxygen transfer to the blood capillaries in a single interlamellar channel is $Q_w\beta(P_{wo} - P_w(l))$, the total oxygen transfer rate in a gill filament having N interlamellar channels is given by $M_o\ Q_w\beta(P_{wo} - P_w(l))N$. Although the lamellar thickness t may depend on the fish species or the maturity of the individual, we assume that $t/d < 1$ and $N\ L/(d+t)\ L/d$, as evidenced by many species such as *Thunnusalbacares*, *Micropterusdolomieu*, and *Raiamontagui* (29, 32).

The stream-wise momentum conservation can be described by the Poiseuille flow solution, $Q_w = Hd^3\Delta P_h/(12\mu l)$, where ΔP_h is the pressure difference applied across the channel (Figure 2.2). Combining this solution with the aforementioned expressions for M_o and P_w, we finally obtained M_o as a function of d and other parameters, including μ, D_w, l, and ΔP_h. Differentiating M_o with respect to d thus yields the optimal interlamellar distances d that maximize M_o:

$$d^4 = 72\frac{\mu D_w l^2}{\Delta P_h}. \tag{2.2}$$

Since mu and D_w are material properties, our model suggests that the optimal lamellar arrangement depends exclusively on the lamellar length l

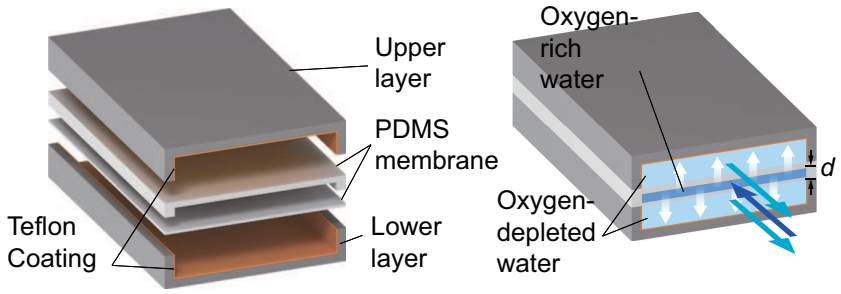

Figure 2.5: Measurement of oxygen transfer rate using a microfluidic chip that mimics a fish gill. A schematic illustration of the PDMS microchannels. Oxygen-rich water passes through the central channel sandwiched by two oxygen-depleted water channels. Oxygen diffuses across the PDMS membranes.

and pumping pressure ΔP_h.

2.3 Experimental validation

We tested the validity of our theory for M_o as a function of d and ΔP_h, by conducting experiments using a microfluidic chip that mimics a fish gill. As shown in Figure 2.5, an engineered gill was constructed of multiple layers of PDMS (polydimethylsiloxane), so that an oxygen-rich water channel was sandwiched between two neighboring channels of counter flowing oxygen-depleted water. Oxygen diffused across the thin PDMS membranes from oxygen-rich to oxygen-depleted water streams, which were pumped into the channels by syringe pumps. Measuring the oxygen concentration at the outlet of the oxygen-rich channel for various channel dimensions and pumping pressures yielded the oxygen transfer rate M_o as a function of d and ΔP_h for the fixed filament length $L = 1$ mm. The results, shown in Figure 2.6, indicate that the empirical measurements support our theory.

2.4 Discussion

Our modeling result, Eq. 2.2, allows us to correlate the lamellar distance and length at a given pumping pressure. Pumping pressures in fish gills primarily depend on the pumping mechanisms.

For most teleost fish using branchial pumping, the pumping pressure is reported to range from 5 to 50 Pa (45). Pelagic teleost fish that typically

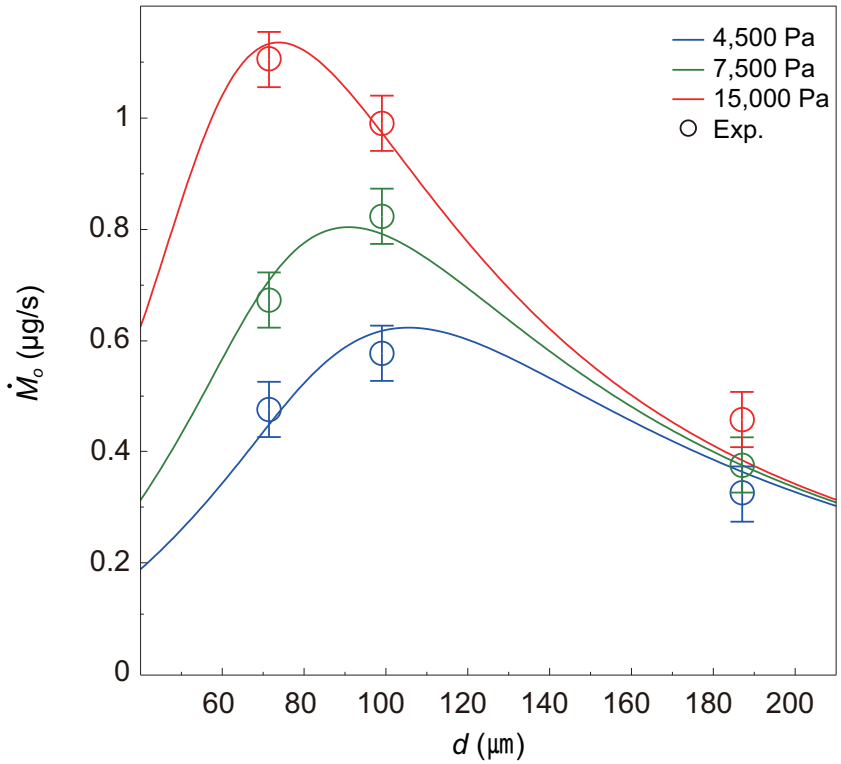

Figure 2.6: Measurement of oxygen transfer rate using a microfluidic chip mimicking a fish gill. The oxygen transfer rate M_o versus the interlamellar distance d for different pumping pressures. The lines and circles correspond to the theoretical predictions and the experimental results, respectively. Characteristic error bars are shown.

employ ram ventilation swim at cruising speeds of $v = 0.7 - 2$ m/s, resulting in a dynamic pressure $(1/2)\rho v^2 \sim$ 0.2-2 kPa, which exceeds branchial pumping pressure (46). Among the species that use ram ventilation, some pelagic elasmobranch fish have developed a unique gill structure called the interbranchial septum; this structure generates primary resistance to water flow, such that only a small fraction of the dynamic pressure on the order of 20 Pa is applied to the interlamellar channels (38).

We compared the proposed model, Eq. 2.2, with biological data (Figure 2.7, Figure 2.8). A comparison of the interlamellar distance versus lamellar length in the gills of 75 species is indicated in Figure 2.7. Most of the data points are clustered within the anticipated interlamellar distance range for each pumping mechanism, which is consistent with our theory. Figure 2.8 shows the correlation between interlamellar distance and body mass. Assuming a geometric similarity across fish species (27), a characteristic body length should be proportional to the cube root of the body mass W. We found that the lamellar length l indeed scales as ${M_b}^{1/3}$, despite the variation in gill shapes (28) (Figure 2.8). On the basis of Eq. 2.2, which predicts that the optimal interlamellar distance d should be scaled as $l^{1/2}$ for a given pressure condition, we obtain $d \sim {M_b}^{1/6}$. This scaling, a very weak dependency of d on M_b, explains the biological data provided in Figure 2.8, and thus reveals the origin of the relatively uniform interlamellar distance over 6 orders of magnitude of body mass.

Our mass-transfer analysis, experiments with a microfluidic chip, and comparison with biological data allowed us to identify the primary evolutionary pressure in gills: maximization of the oxygen transfer rate for a given pumping pressure. The optimum is reached at an interlamellar distance that increases the surface area for oxygen diffusion but does not markedly impede water flow. The morphology of fish gills exemplifies the natural design strategy, whereby size change is accommodated by proliferation of the exchange surface, and not by alteration of the basic size and geometry of the exchange unit. Similar examples can be found in other biological systems, such as blood capillary size (27), red blood cell size (27), and the choanocytic system of calcareous sponges (47). This natural optimization strategy found in fish demonstrates how the control of channel arrangement in microfluidic devices enhances heat and mass transfer, a critical issue faced in many practical situations, including micro-heat exchangers (48) and lab-on-a-chip systems for drug delivery (49) and biochemical analysis (50).

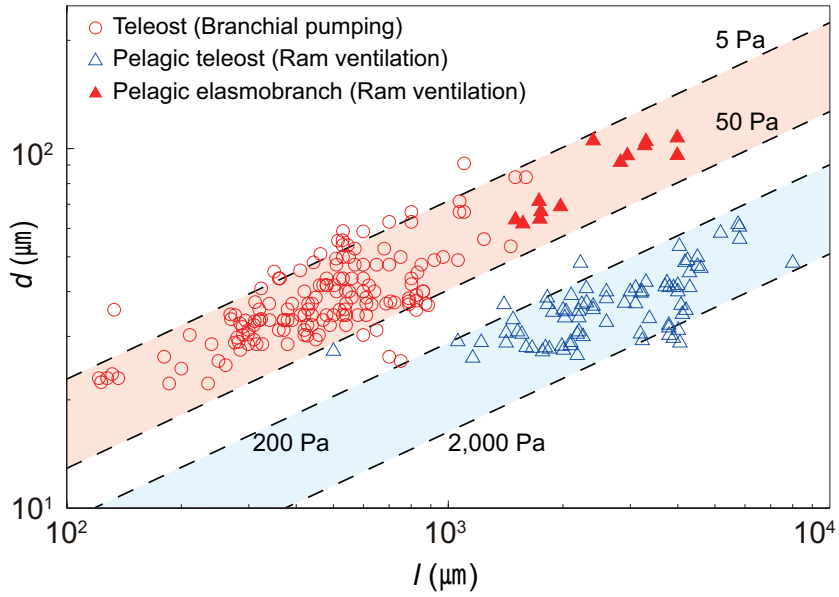

Figure 2.7: Biological data on the lamellar dimensions of fish gills. The dependence of interlamellar distance on lamellar length. The dotted lines indicate the range of optimal conditions depending on the pumping pressure. The pumping pressures for fish using branchial pumping and for pelagic teleost fish using ram ventilation range typically from 5 to 50 Pa (45) and 0.2 to 2 kPa (46), respectively; for pelagic elasmobranch fish using ram ventilation but having interbranchial septa, the applied pressure for the interlamellar channel is approximately 20 Pa (38).

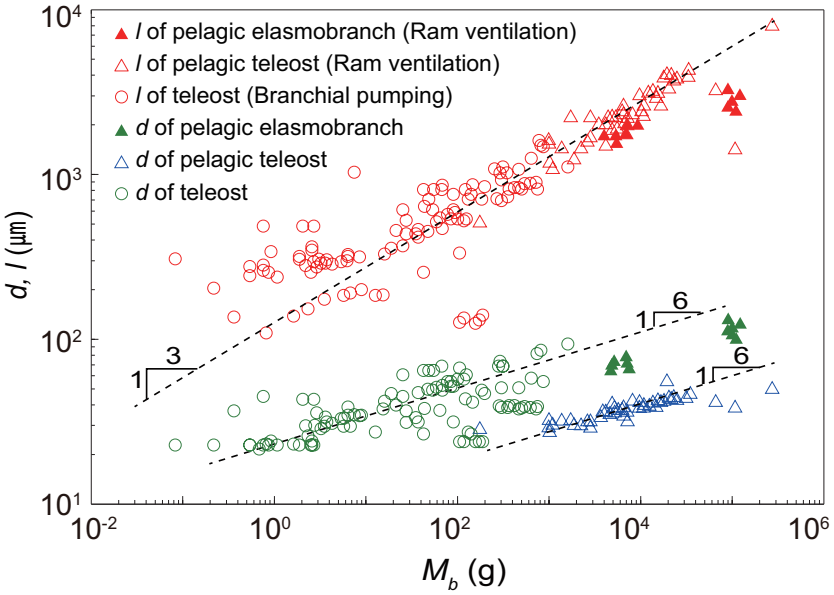

Figure 2.8: Biological data on the lamellar dimensions of fish gills. The dependence of the lamellar length and interlamellar distance on the body mass. Owing to the geometric similarity of fish species, the lamellar length l scales as $l \sim {M_b}^{1/3}$; combining the scaling with our models prediction, $d \sim l^{1/2}$, yields $d \sim {M_b}^{1/6}$.

2.5 Materials and Methods

2.5.1 Mass-transfer experiments an engineered gill

We fabricated an engineered gill system consisting of PDMS microchannels, where gas transfer occurs across the membranes separating the channels. The PDMS structure was constructed using a 10 : 1 mixture of Sylgard-184 (Dow Corning) cured by baking for 30 min at 80 °C in a vacuum oven. We coated the inner wall of the upper and lower layers with 0.6 wt% Teflon-AF (DuPont 601S2 and 3M Fluorinert Electronic Liquid FC40) to prevent oxygen diffusion out of the channels. All three channels had identical widths of 2 mm and lengths of 70 mm. The membrane thickness was 20 μm. We changed the height of the central channel from 70 to 190 μm, whereas the heights of the other channels were fixed at 200 μm. In order to avoid adhesion between two membranes and membrane rupturing. As shown in Figure 2.9, our microfluidic chip has micro pillar structures in microchannels to support two thin membranes. Sodium sulfite was used to control the concentration of dissolved oxygen in water. Channel flow was achieved using a syringe pump (Harvard PHD 22/2000). Reynolds numbers range from 0.002 to 0.3, and the flow is laminar. An oxygen microsensor (Unisense OX-100) was used to measure the partial pressure of oxygen at the outlet of the central channel.

2.5.2 Scanning electron microscopy

The gill of a rockfish, *Sebastes schlegelii*, was fixed in Karnovsky fixative solution and then in 2% osmium tetroxide in a 0.1 M cacodylate buffer. The specimen was dried in a drying device (Baltzer CPD030) after partial dehydration using a graded ethanol series. The dried specimen was coated with a thin layer of platinum in a sputter coater (Bal-Tec SCD005) and examined using a Field-Emission Scanning Electron Microscope (Carl Zeiss SUPRA 55VP).

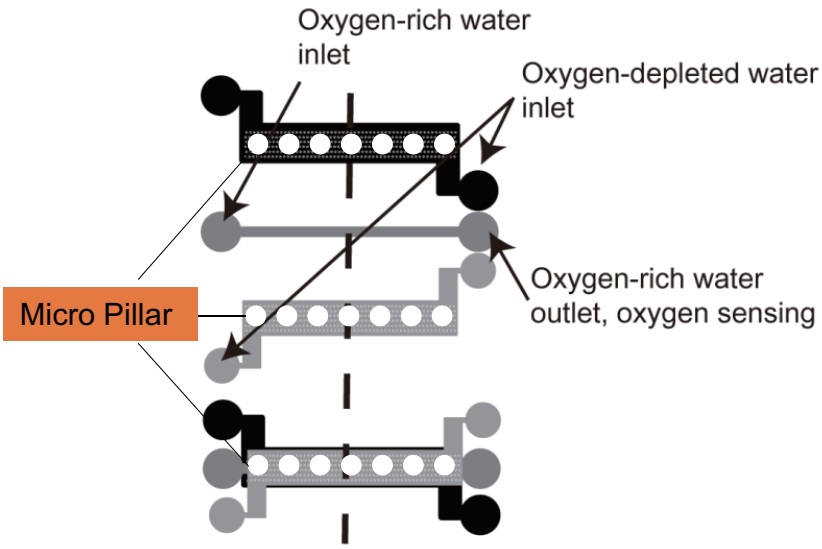

Figure 2.9: Design of microfluidic chips which mimics a fish gill. Three layers of microchannels are separated by thin PDMS membrane which thickness is order of 10 μm. Micro pillar structures in water channel prevent two membranes from adhesion and rupturing. Oxygen partial pressure is measured at the outlet of oxygen rich water channel.

Chapter 3

Physical principle of acinar airway design in human lungs

3.1 Introduction

The transport network systems in nature play an important role in the survival and growth. These systems are found in both plants (51-55) and human body (56-62). Additionally, these systems perform different functions such as transporting nutrients or water, and delivering oxygen to blood. For these transport networks, one may expect that the transport efficiency would be dependent on the geometry of the network, leading us to question what the design principle of the transport network systems are in nature (52, 63-65).

In 1926, Dr. Murray investigated the design principles for blood vascular networks, which branch with a systematic reduction in diameter. Specifically, he studied what determines the diameter reduction ratio in vascular networks. The idea, called Murrays law, was that blood vascular networks aim to minimize the energy cost of a given blood flow. Moreover, this law suggests that the cost of blood flow in the vasculature is principally determined by the viscous dissipation and metabolic energy of living cells in blood, which depends on the diameter reduction ratio. If the reduction ratio is low, the diameter of the daughter branches becomes small, resulting in highly viscous dissipation. In contrast, if the reduction ratio is high, the diameter of the daughter branches becomes large. Consequently, blood volume increases, necessitating a large amount of metabolic energy output for

living cells in the blood. Hence, an optimal diameter reduction ratio exists for minimizing the energy cost of blood flow; as Murray demonstrated, the optimal reduction ratio is 0.79 (59, 64, 66).

3.2 Theoretical analysis

Murrays law is applicable to human lung airways that branch by dichotomy with a systematic diameter reduction as shown in Figure 3.1 (60, 61, 66-69). Similar to blood vascular networks, the diameter reduction ratio should not be too small in order to avoid high viscous dissipation. In human breathing, the volume of a single inhalation of air is limited. Therefore, the volume of the airway needs to be small to maximize the transportation of air to the alveoli where oxygen exchange occurs. Consequently, the optimal diameter reduction ratio will minimize the energy cost by viscous dissipation in airways, and this analysis yields the same result for optimal diameter reduction ratio, 0.79. However, as shown in the Figure 3.2, the diameter reduction ratio is consistent with Murrays law up to the 15th generation, within the conducting airways. (66-72)

Interestingly, in acinar airways, with the generation number is higher than 16, the reduction ratio is clearly different from that of the conducting airways, which obey Murrays law as shown in Figure 3.2 (69). Most previous studies of diameter reduction ratios in the acinar airways have suggested that airways that are slightly larger than those predicted by the diameter reduction ratio of the conducting airways provide the system with a safety margin with respect to resistance (61, 68). Additionally, some studies have indicated that the differences between the two diameter reduction ratios arise from their different transport mechanisms (59). In conducting airways, as is observed in the blood vasculature, oxygen transport is driven by advection with viscous dissipation. However, in acinar airways, diffusion is the predominant to oxygen transport mechanism (68, 73). Thus, we rationalize the diameter reduction ratio of acinar airways by considering the mechanism of acinar airway transport, i.e., diffusion.

In acinar airways, where diffusion is the dominant transport mechanism, the largest diameter reduction ratio may be considered an optimal design for transporting due to the increased total cross-sectional area of the airways for diffusion transport. However, obviously, the largest diameter reduction ratio would not be the optimal design, and the energy cost of the acinar airways should also be considered, similar to the design of the blood vasculature. The larger the diameter reduction ratio, the more energy is metabolically required to maintain the acinar airways(59). In order to es-

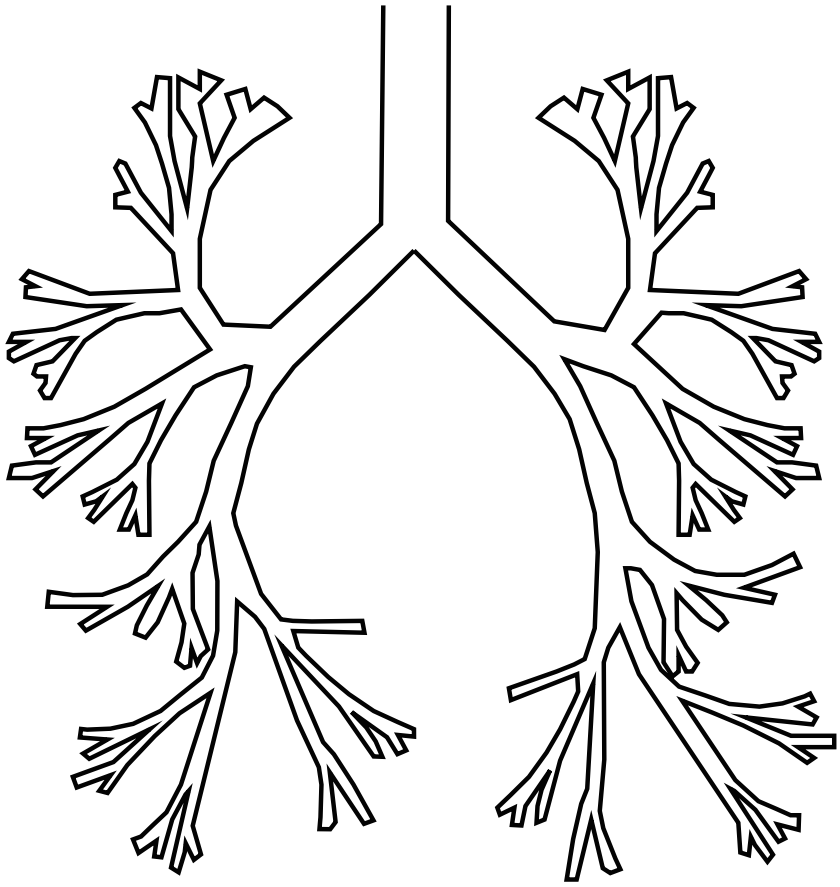

Figure 3.1: General topography of Lung structures. The airways consist of the hierarchy of branchial trees.

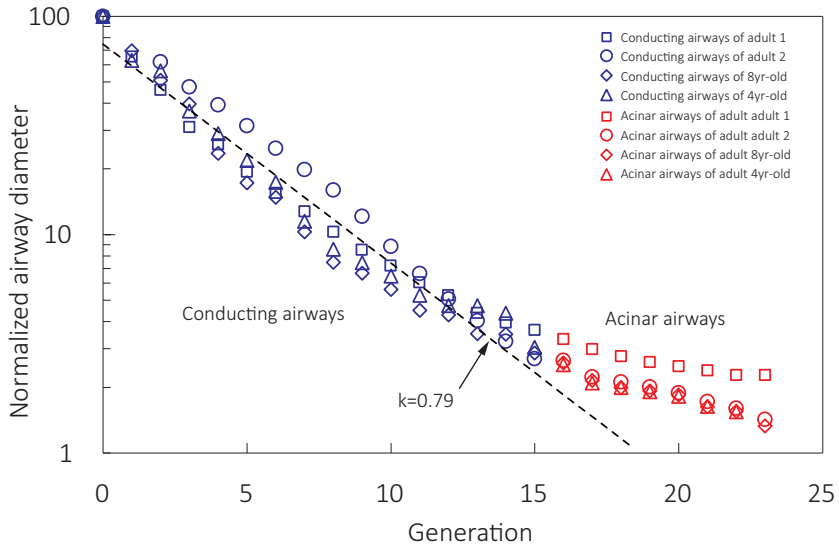

Figure 3.2: Normalized diameter of conducting airways and acinar airways versus generation. Diameter reduction of conducting airways obeys Murrays law which represents the optimal diameter reduction ratio is 0.79, whereas the acinar airways are reduced to a less steeply. The diameter reduction ratio of acinar airways is 0.94. Data were taken from Heafeli-Bleuer and Weibel (1988) and Finlay *et al.* (2000)

timate the energy cost of acinar airways, we assumed that the energy cost of the acinar airways is proportional to the total surface area of the acinar airways(74) because the acinar airways consist of a layer of epithelial cells. Thus, we suggest that the optimal diameter reduction ratio of the acinar airways would minimize the energy cost for maintenance of these airways for oxygen transport, as required by metabolic demand. Here, we develop a mathematical model for diffusion transport within the acinar airways and reveal the origin of the observed diameter reduction ratio in acinar airways.

3.3 Mathematical model

Because the diffusion transfer rate is given by Ficks law, the oxygen transfer rate is proportional to the cross-sectional area of acinar airways and the oxygen concentration gradient. By noting that the duct boundaries would not affect diffusion, arranging all the ducts for each generation side by side does not change the oxygen transfer rate. Therefore, the airways can be simplified as a diverging duct, which allows us to write $A(x) = A_{16}\exp(ax)$, $a = \ln(2k^2)/l$, where $A(x)$ is the total cross-sectional area of acinar airway along the generation axis, A_{16} is total cross-sectional area of the acinar airways of the 15th generation, k is the diameter reduction ratio, and l is the single duct length.

For an infinitesimal control volume, as shown in Figure 3.3, the conservation of oxygen can be written as $(\partial\phi/\partial t)A(x) = q''(x)A(x) - q''(x + \Delta x)A(x + \Delta x)$, where ϕ is the partial pressure in the acinar airways, t is time, and q'' is the oxygen flow rate per unit cross-sectional area. $q''(x+\Delta x)$ and $A(x + \Delta x)$ can be written as $q''(x + \Delta x) = q''(x) + (\partial q''(x)/\partial x)\Delta x$ and $A(x + \Delta x) = A(x) + (\partial A(x)/\partial x)\Delta x$, respectively. The oxygen flow rate per unit cross sectional area can be expressed using Ficks first law as $q''(x) = -D(\partial\phi/\partial x)$, where D is the oxygen diffusion coefficient in air. This allows us to write,

$$\frac{\partial\phi}{\partial t} = D\left(\frac{\partial^2\phi}{\partial x^2} + \alpha\frac{\partial\phi}{\partial x}\right). \tag{3.1}$$

In order to solve this unsteady partial differential equation (3.1), we need an initial and two boundary conditions. When inhalation begins, we assume that the oxygen concentration of the acinar airways is the same as that of the blood capillary, because all of the oxygen has been diffused to the capillaries. This allows us to write the initial condition as $\phi(x, 0) = \phi_{capillary}$, where $\phi_{capillary}$ is the oxygen concentration of the blood capillary. We further assume that during the inspiration, oxygen concentration of

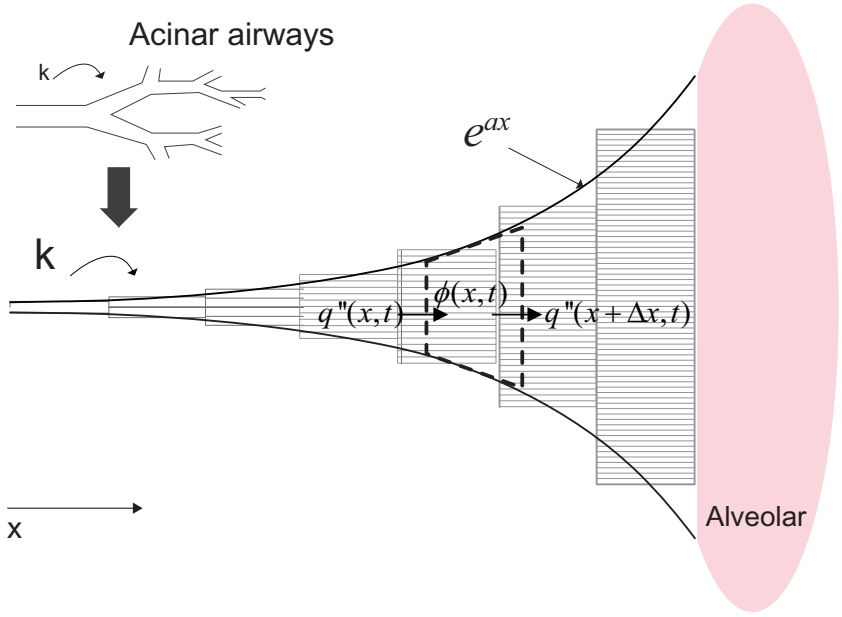

Figure 3.3: A schematic illustration of surface area of acinar airways with generation developing. Acinar airways are consist of series of ducts and alveolar. Because oxygen transfer in acinar airways is driven by diffusion. Arranging all the duct for each generation side by side does not change the oxygen transfer rate. Thus the acinar airways can be simplified as a diverging duct, and we assume the diverging duct with an exponential function in terms of constant a, which depends on the diameter reduction ratio and single duct length.

the entrance to the acinar airways is equal to that of fresh air due to the supply of fresh air from conducting airways. Therefore, the first boundary condition is given as $\phi(0,t) = \phi_{air}$, where ϕ_{air} is the oxygen concentration of air. When we examine the end of the acinar airways, oxygen diffuses to capillaries across the alveolar membrane and the second boundary condition is given by the continuity of oxygen which yields,

$$-DA(L)\left(\frac{\partial\phi(x,t)}{\partial x_{x=L}}\right) = D_w A_{alveoli}\left(\frac{\phi(L,t)-\phi_{capillary}}{e}\right) \tag{3.2}$$

where D_w is the oxygen diffusion coefficient of water, $A_{alveoli}$ is the total surface area of alveoli, and e is the thickness of the alveolar membrane.

We nondimensionalize the oxygen transfer equation (3.1), the boundary and initial conditions (3.2) by using dimensionless variable $x^* = xL$, $t^* = t/\tau$, $\phi^* = (\phi-\phi_0)/(\phi_1-\phi_0)$, $D^* = D\tau/L^2$, $A^* = aL/A$ and $h^* = (D_w A_\infty L)/(DA_1 e)$:

$$\frac{\partial\phi^*}{\partial t^*} = D\left(\frac{\partial^2\phi^2}{\partial x^{*2}} + A^*\frac{\partial\phi^*}{\partial x}\right), \tag{3.3}$$

$$\phi^*(0,t^*) = 0,\ h^*\phi^*(1,t^*) + \frac{\partial\phi^*(1,t^*)}{\partial x^*} = 0,\ \phi^*(x^*,0) = 0. \tag{3.4}$$

The problem is solved by a superposition

$$\phi^*(x,t^*) = {\phi_H}^*(x^*,t^*) + {\phi_{SS}}^*(x^*) \tag{3.5}$$

where ${\phi_H}^*(x^*,t^*)$ is the transient, homogeneous solution that takes the homogeneous boundary conditions and where ${\phi_{SS}}^*$ is the steady-state solution that takes the nonhomogeneous boundary condition. This formulation yields

$$\frac{\partial{\phi_H}^*}{\partial t^*} = D^*\left(\frac{\partial^2{\phi_H}^*}{\partial x^{*2}} + A^*\frac{\partial{\phi_H}^*}{\partial x^*}\right), \tag{3.6}$$

$${\phi_H}^*(0,t^*) = 0,\ h^*{\phi_H}^*(1,t^*) + \frac{\partial{\phi_H}^*(1,t^*)}{\partial x^*} = 0,\ {\phi_H}^*(x^*,0) = -{\phi_{SS}}^*(x^*) \tag{3.7}$$

for the transient solution and

$$\frac{d^2{\phi_{SS}}^*}{dx^{*2}} + A^*\frac{d{\phi_{SS}}^*}{dx^*} = 0,\ {\phi_{SS}}^*(0) = 1,\ h^*{\phi_{SS}}^*(1) + \frac{d{\phi_{SS}}^*(x^*=1)}{dx^*} = 0 \tag{3.8}$$

For the steady-state solution. The ODE of equations (3.8) yields

$$\phi_{SS}{}^*(xx^*) = \frac{h^* e^{-A^* x^*} - (h^* - A^*)e^{-A^*}}{h^* - (h^* - A^*)e^{-A^*}} \tag{3.9}$$

The transient problem of equations, boundary conditions and initial condition are transformed using

$$\phi_{SS}{}^*(xx^*) = W(x^*, t^*) \exp\left(-\frac{A^*}{2}x^* - \frac{D^*(A^*)^2}{4}t^*\right). \tag{3.10}$$

We have the boundary value problem

$$\frac{\partial w}{\partial t} = D^* \frac{\partial^2 w}{\partial {x^*}^2},\ w(0,t^*) = 0,\ H^* w(1,t^*) + \frac{\partial w(1,t^*)}{\partial x^*} = 0,$$
$$w(x^*,0) = -\phi_{SS}{}^*(x^*) \exp\left(\frac{A^*}{2}x^*\right) \tag{3.11}$$

where, $H^* = h^* - A^*/2$. For that does have two-point boundary conditions leading to a Sturm-Liouvile problem. By assuming a product solution $w(x^*, t^*) = X(x^*)T(t^*)$ of the homogeneous conditions in problem (3.11), we see that

$$X'' + \lambda X = 0,\ X(0) = 0,\ H^* X(1) + X'(1) = 0\ (H^* > 0) \tag{3.12}$$

and $T' + D^* \lambda T = 0$. The Sturm-Liouville problem (3.12) has the eigenvalues and normalized eigenfunctions

$$\lambda_n = {\beta_n}^2,\ X_n(x) = \Phi_n(x^*) = \sqrt{\frac{2H^*}{H^* + (\cos\beta_n)^2}} \sin\beta_n x^* \tag{3.13}$$

where $\tan\beta_n = -\beta_n / H^*$ and the corresponding functions of t are

$$T_n(t^*) = e^{-D^* {\beta_n}^2 t^*} \tag{3.14}$$

hence,

$$w(x^*, t^*) = \sum_{n=1}^{\infty} c_n e^{-D^* {\beta_n}^2 t^*} \Phi_n(x^*). \tag{3.15}$$

We may find the coefficients in the expansion,

$$\phi_{SS}(x^*) \exp\left(\frac{A^*}{2}x^*\right) = \sum_{n=1}^{\infty} c_n \Phi_n(x^*) \tag{3.16}$$

by writing

$$c_n = (w(x^*,0),\phi_n) = \frac{1}{h^* - (h^* - A^*)e^{-A}}\sqrt{\frac{2H^*}{H^* + (\cos\beta_n)^2}}$$
$$\times \int_0^1 (h^* - A^*)e^{-A^* + \frac{A^*}{2}x^*}\sin\beta_n x^* - h^* e^{-\frac{A^*}{2}x^*}\sin\beta_n x^* dx^*$$
$$= \frac{1}{h^* - (h^* - A^*)e^{-A^*}}\sqrt{\frac{2H^*}{H^* + (\cos\beta_n)^2}}\frac{1}{\left(\frac{A^*}{2}\right)^2 + {\beta_n}^2}$$
$$\times \left[e^{-\frac{A^*}{2}}\left((2h^* - A^*)\frac{A^*}{2}\sin\beta_n + A^*\beta_n\cos\beta_n\right) + e^{-A^*}(h^* - A^*)\beta_n - h^*\beta_n\right]. \tag{3.17}$$

After substituting these values of c_n into expression (3.15) and then simplifying and combining the result with expression (3.9), as indicated in equation (3.5), we find the oxygen concentration function in acinar airways:

$$\phi^*(x^*,t^*)\frac{h^* e^{-A^* x^*} - (h^* - A^*)e^{-A^*}}{h^* - (h^* - A^*)e^{-A^*}}$$
$$+e^{-\frac{A^*}{2}x^*}\sum_{n=1}^{\infty} c_n\sqrt{\frac{2H^*}{H^* + (\cos\beta_n)^2}}\sin\beta_n x^* e^{-D^*\left[\left(\frac{A^*}{2}\right)^2 + {\beta_n}^2\right]t^*} \tag{3.18}$$

where, $\tan\beta_n = -\beta_n/H^*$.

In expression (3.18), the first term on the right side means the steady solution of oxygen concentration function. When we look at the second term on the right side, the unsteady solution of oxygen concentration function would be diminished with increasing of time.

3.4 Discussion

We assumed that similar to blood vasculature, the energy cost of the acinar airways is proportional to the volume of cells within the acinar airways. However, unlike the blood vasculature, the volume of cells within the acinar airways is proportional to the total surface area of the acinar airways, $\sum A$, because acinar airway and alveolar tissues consist of a layer of epithelial cells. Direct measurements indicate that the total surface area of alveoli is in the order of 60 m^2 (69). Thus, we can estimate the total surface area of the acinar airways, which consist of airway ducts and alveoli.

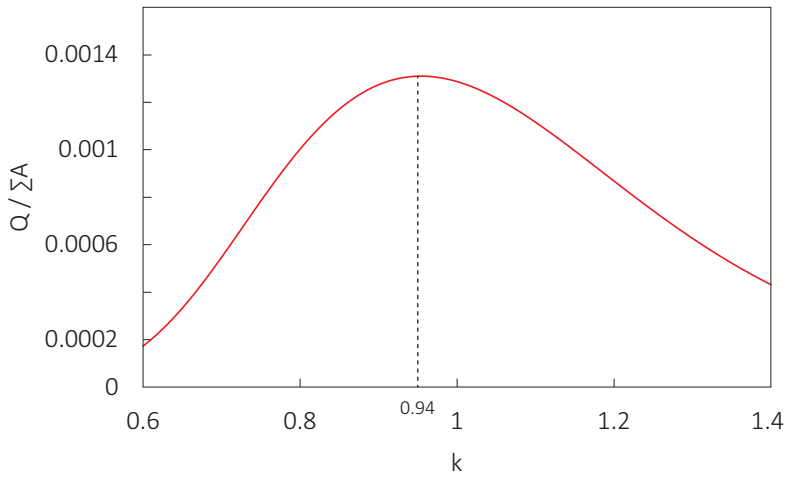

Figure 3.4: The oxygen transfer rate per total surface area of acinar airways ($Q/\sum A$). We assume that the surface area of acinar airway is proportional to the energy cost of acinar airways, because acinar airways consist of a layer of epithelium cell. In this figure, the maximum value of oxygen transfer rate per total surface area suggests that the optimal diameter reduction ratio of acinar airways for minimizing energy cost for a given amount of oxygen transport is 0.94.

Combining our oxygen transfer rate modeling results and the total surface area of acinar airways allows us to correlate the oxygen transfer rate per total surface area of acinar airways with the diameter reduction ratio. As shown in Figure 3.4, the oxygen transfer rate per total surface area of acinar airways suggests that the optimal reduction ratio for minimizing the energy cost of acinar airways for oxygen transfer is 0.94. Consequently, we found that our hypothesis was well consistent with the observed reduction ratio of acinar airways.

According to our theoretical result, if the diameter reduction ratio of acinar airways is the same as that of the conducting airways, the energy cost of acinar airways for a given oxygen transport amount increases more than 30% compared to the optimal reduction ratio because the oxygen transfer rate decreases faster than the energy cost of acinar airways. In contrast, if the diameter reduction ratio of acinar airways is larger than the optimal reduction ratio, the energy cost of the acinar airways increases faster than the oxygen transfer rate. When we consider that physiological variability

of actual lungs is 7% (61), the energy cost of the acinar airways for a given oxygen transport amount increases 6%.

In summary, we identified the primary evolutionary pressure in the acinar airways of the lungs: minimization of the energy cost of acinar airways for a given oxygen transport amount by metabolic demands. The larger diameter of the acinar airways enhances the oxygen transfer rate because of reduced diffusion resistance; however the energy cost of the acinar airways is increased, so the efficiency of the acinar airways is lower. In this respect, branching of acinar airways is closely related to Murrays law, similar to that of conducting airways. Similar examples can be found in other biological and industrial systems(75), water transport system in plants(52, 63), and vascular networks in multifunctional materials(76). This natural optimization strategy found in the acinar airways of the lung demonstrates how the control of branching in microfluidic devices enhances diffusion(77-79).

3.5 Future work: Experimental validation

In order to validate our mathematical model of transportation of oxygen in acinar airways, mass transfer experiments on engineered lung systems are required. As shown in Figure 3.5, engineered lung systems would be consist of oxygen rich air chamber, dichotomy branched airways with systemic diameter reduction and sodium sulfite solution chamber and be constructed by PDMS. The PDMS structures can be prepared by using a $10:1$ mixture of Sylgard-184 (Dow Corning) cured by baking for 30 min at $80\,^{\circ}\mathrm{C}$ in a vacuum oven. Inner wall of engineered lung would be coated with 0.6 $wt\%$ Teflon-AF (DuPont 601S2 and 3M Fluorinert Electronic Liquid FC40) to prevent oxygen diffusion out of the channels. In the engineered lung systems, oxygen diffuses from oxygen rich air chamber to sodium sulfite solution chamber through dichotomy branched airways. Sodium sulfite solution can mimic the pulmonary artery because sodium sulfite reacts with the oxygen from airways similar to hemoglobin in bloods of the pulmonary artery. The diameter reduction ratio of airways, which represents the upper airway diameter divided by the lower airway diameter, is supposed to change from 0.6 to 1. The oxygen transfer rate can be measured by using oxygen microsensor (Unisense OX-100). We expect that the oxygen transfer rate in engineered lung systems increases with the diameter reduction ratio thanks to increasing of cross sectional area.

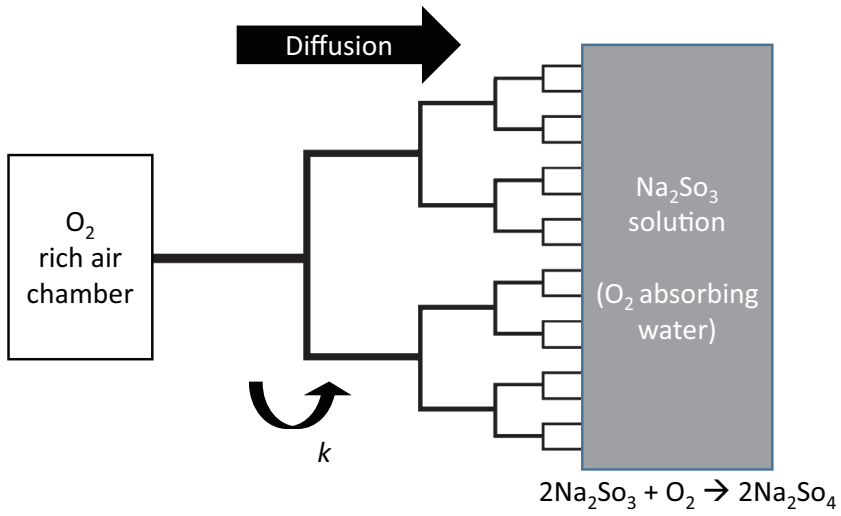

Figure 3.5: Schematic illustration of engineered lung systems. Engineered lung systems consist of oxygen rich air chamber, dichotomy branched airways with systemic diameter reduction and sodium sulfite solution chamber. In this microfluidic devices, oxygen diffuses from oxygen rich air chamber to sodium sulfite solution through airways.

Chapter 4

Conclusions

We have explored two respiration systems: fish gills and human lungs. We have rationalized two respiration strategies for mass transport and demonstrated that these strategies are optimized for efficient respiration. Thus, we developed a general framework for optimal design principles in respiration systems in air and under water.

In Chapter 2, we showed that interlamellar distances changed only slightly, despite a huge variation in fish size. We also identified the dominant constraints and suggested a physical design principle for each pumping mechanism in fish, thereby rationalizing the interlamellar distances of a variety of species of fish. Simple mathematical modeling arguments were validated by experiments with microfluidic chips that mimic the structures fish gills. The optimum is reached at an interlamellar distance that increases the surface area for oxygen diffusion but does not markedly impede water flow. The morphology of fish gills exemplifies the natural design strategy, whereby size change is accommodated by proliferation of the exchange surface, and not by alteration of the basic size and geometry of the exchange unit.

There are two dominant oxygen transport mechanisms in human lung airways: advection and diffusion. We suggested that systematic diameter reduction ratios in conducting and acinar airways depend on their dominant transport mechanisms. Similar to the blood vasculature, we assumed that the energy cost of acinar airways is proportional to the volume of cells within acinar airways. The large diameter reduction ratio of acinar airways increases the oxygen transfer rate, which is driven by diffusion. However, it also provides a large surface area for the acinar airways, which results in a huge energy cost for the acinar airways. Thus, our model enables us to rationalize the observed reduction ratio while considering the metabolic

energy cost of airways, suggesting a modified Murrays law for acinar airways.

Comparison the design principle between fish gills and human lungs gives us thoughtful insight in evolutionary pressure depending respiration fluids either water or air. As we mentioned above, water has far greater density and viscosity the air. The density ratio of water to air is 1000 and the viscosity ratio of water to air is 100. If the lungs use water as respiration fluid, mammals need 1000 times greater energy to pump respiration fluid through airways. Moreover, because the pulsation of respiration flow is critically affected by the density, respiration of lungs through water flow would consume more energy than we expected. Unlike mammalian lungs, fish gills not only either have two muscle pumps or use dynamic pump caused by swimming to flow the water through lamellar channel, but also have operculum that makes unidirectional respiration flow. Thanks to unidirectional respiration flow, fish gills could use only half energy when we compare with reciprocation respiration flow.

However, unidirectional respirational flow is not always good for animals. The first reason is that operculum makes exposing of membrane layer of respiration systems on outside easy. Natural enemy in nature can easily overpower the animals by attacking operculum. Moreover, the lamellar structures for uniform flow is so weak to withstand to the dry air unlike lung airways that have conducting airways to prevent the dehydration of acinar airways. When we consider respiration in the air, uniform flow achieved by operculum and dual pump needs to much energy to maintain respiration systems because air can be easily controlled only using single pump. Thus, ground animals saved the energy for respiration by using air as respiration fluids and the saved energy makes ground animals evolve more complex and higher.

Consequently, respiration systems in nature have been optimizing small-scale oxygen transport strategies for millions of years, while man has only recently become interested in micro-scale heat and fluid transportation, for applications such as drug delivery, microheat exchangers, and the biomolecule handling. Although biomimicry is now a central methodology used in engineering sciences, we expect that the optimal design principles of fish gills and human lungs for fluid transport driven by diffusion will prompt further biomimetic technological advances.

Appendix A

Supplementary tables

Table A1. Dimensions of gill and body weight of fish.

Genus	Family	Classification[a]	Weight [g]	d [µm][b]	l [µm][c]	Reference
Oryzias	Adrianichthyidae	*T.*	179	23	137	(*37*)
Oryzias	Adrianichthyidae	*T.*	166	23	128	"
Oryzias	Adrianichthyidae	*T.*	150	23	121	"
Oryzias	Adrianichthyidae	*T.*	112	23	131	"
Oryzias	Adrianichthyidae	*T.*	100	23	123	"
Alopias	Alopiidae	*P.E.*	100,000	107	3,987	(*31*)
Anabas	Anabantidae	*T.*	6	37	312	(*80*)
Anabas	Anabantidae	*T.*	15	41	324	"
Anabas	Anabantidae	*T.*	24	43	362	"
Anabas	Anabantidae	*T.*	35	46	409	"
Anabas	Anabantidae	*T.*	45	48	444	"
Anabas	Anabantidae	*T.*	56	49	508	"
Anabas	Anabantidae	*T.*	65	51	462	"
Anabas	Anabantidae	*T.*	74	54	533	"
Anabas	Anabantidae	*T.*	80	54	529	"
Anabas	Anabantidae	*T.*	96	56	529	"
Anabas	Anabantidae	*T.*	112	55	514	"
Anabas	Anabantidae	*T.*	118	59	530	"
Callionymus	Callionymidae	*T.*	64	67	800	(*29*)
Callionymus	Callionymidae	*T.*	46	63	700	"
Callionymus	Callionymidae	*T.*	24	59	600	"
Trachurus	Carangidae	*T.*	12	26	180	"
Trachurus	Carangidae	*T.*	40	26	250	"
Trachurus	Carangidae	*T.*	125	26	700	"

Trachurus	Carangidae	*T.*	135	26	750	"
Carcharhinus	Carcharhinidae	*P.E.*	100,000	92	2,827	(*31*)
Prionace	Carcharhinidae	*P.E.*	100,000	105	3,299	"
Carcharhinus	Carcharhiniformes	*P.E.*	100,000	96	2,949	"
Micropterus	Centrarchidae	*T.*	0	36	133	(*29*)
Micropterus	Centrarchidae	*T.*	3	35	269	"
Micropterus	Centrarchidae	*T.*	26	36	520	"
Micropterus	Centrarchidae	*T.*	41	37	630	"
Micropterus	Centrarchidae	*T.*	116	42	800	"
Micropterus	Centrarchidae	*T.*	189	45	830	"
Micropterus	Centrarchidae	*T.*	289	49	920	"
Micropterus	Centrarchidae	*T.*	452	49	1,060	"
Micropterus	Centrarchidae	*T.*	618	56	1,240	"
Micropterus	Centrarchidae	*T.*	838	54	1,460	"
Chaenocephalus	Channichthyidae	*T.*	750	83	1,600	"
Chaenocephalus	Channichthyidae	*T.*	790	83	1,500	"
Astatoreochromis	Cichlidae	*T.*	-	37	430	(*81*)
Bathybates	Cichlidae	*T.*	-	31	650	"
Boulengerochromis	Cichlidae	*T.*	-	34	540	"
Callochromis	Cichlidae	*T.*	-	48	510	"
Cardiopharynx	Cichlidae	*T.*	-	43	560	"
Cyatopharynx	Cichlidae	*T.*	-	40	510	"
Cyatopharynx	Cichlidae	*T.*	-	53	680	"
Cyatopharynx	Cichlidae	*T.*	-	50	530	"
Cyatopharynx	Cichlidae	*T.*	-	48	570	"
Cyrtocara	Cichlidae	*T.*	-	34	410	"
Docimodus	Cichlidae	*T.*	-	43	800	"

Haplochromis	Cichlidae	*T.*	-	24	200	"
Haplochromis	Cichlidae	*T.*	-	29	240	"
Haplochromis	Cichlidae	*T.*	-	31	300	"
Haplochromis	Cichlidae	*T.*	-	32	310	"
Haplochromis	Cichlidae	*T.*	-	33	320	"
Haplochromis	Cichlidae	*T.*	-	30	290	"
Haplochromis	Cichlidae	*T.*	-	34	270	"
Haplochromis	Cichlidae	*T.*	-	37	340	"
Haplochromis	Cichlidae	*T.*	-	34	270	"
Haplochromis	Cichlidae	*T.*	-	33	370	"
Haplochromis	Cichlidae	*T.*	-	33	370	"
Haplochromis	Cichlidae	*T.*	-	42	480	"
Haplochromis	Cichlidae	*T.*	-	36	380	"
Haplochromis	Cichlidae	*T.*	-	36	320	"
Haplochromis	Cichlidae	*T.*	-	31	370	"
Haplochromis	Cichlidae	*T.*	-	37	390	"
Haplochromis	Cichlidae	*T.*	-	34	480	"
Haplochromis	Cichlidae	*T.*	-	33	380	"
Haplochromis	Cichlidae	*T.*	-	31	360	"
Haplochromis	Cichlidae	*T.*	-	31	420	"
Haplochromis	Cichlidae	*T.*	-	32	440	"
Haplochromis	Cichlidae	*T.*	-	33	370	"
Haplochromis	Cichlidae	*T.*	-	43	520	"
Haplochromis	Cichlidae	*T.*	-	40	540	"
Haplochromis	Cichlidae	*T.*	-	34	500	"
Haplochromis	Cichlidae	*T.*	-	43	530	"
Haplochromis	Cichlidae	*T.*	-	33	470	"

Haplochromis	Cichlidae	*T.*	-	42	470	"
Haplochromis	Cichlidae	*T.*	-	42	500	"
Haplochromis	Cichlidae	*T.*	-	34	420	"
Haplochromis	Cichlidae	*T.*	-	40	550	"
Haplochromis	Cichlidae	*T.*	-	40	600	"
Haplochromis	Cichlidae	*T.*	-	43	600	"
Hemibates	Cichlidae	*T.*	-	29	450	"
Hemitilapia	Cichlidae	*T.*	-	48	650	"
Hoplotilapia	Cichlidae	*T.*	-	38	610	"
Lamprologus	Cichlidae	*T.*	-	32	490	"
Lamprologus	Cichlidae	*T.*	-	34	580	"
Lamprologus	Cichlidae	*T.*	-	38	560	"
Lamprologus	Cichlidae	*T.*	-	30	420	"
Lamprologus	Cichlidae	*T.*	-	40	640	"
Lamprologus	Cichlidae	*T.*	-	32	540	"
Lethrinops	Cichlidae	*T.*	-	53	570	"
Limnochromis	Cichlidae	*T.*	-	42	620	"
Macropleurodus	Cichlidae	*T.*	-	37	540	"
Petrochromis	Cichlidae	*T.*	-	40	420	"
Petrochromis	Cichlidae	*T.*	-	50	970	"
Platytaeniodus	Cichlidae	*T.*	-	36	430	"
Pseudotropheus	Cichlidae	*T.*	-	29	380	"
Pungu	Cichlidae	*T.*	-	33	390	"
Rhamphochromis	Cichlidae	*T.*	-	34	530	"
Simochromis	Cichlidae	*T.*	-	34	610	"
Simochromis	Cichlidae	*T.*	-	37	610	"
Thoracochromis	Cichlidae	*T.*	-	30	210	"

Thoracochromis	Cichlidae	*T.*	-	37	440	"
Tropheus	Cichlidae	*T.*	-	29	310	"
Tropheus	Cichlidae	*T.*	-	34	440	"
Xenotilapia	Cichlidae	*T.*	-	43	360	"
Xenotilapia	Cichlidae	*T.*	-	42	460	"
Clupea	Clupeidae	*T.*	85	30	600	(*29*)
Clupea	Clupeidae	*T.*	51	48	600	"
Lepidocephalichthys	Cobitidae	*T.*	3	28	285	(*82*)
Lepidocephalichthys	Cobitidae	*T.*	4	30	298	"
Lepidocephalichthys	Cobitidae	*T.*	4	30	280	"
Lepidocephalichthys	Cobitidae	*T.*	5	32	290	"
Lepidocephalichthys	Cobitidae	*T.*	6	33	320	"
Lepidocephalichthys	Cobitidae	*T.*	7	34	324	"
Coryphaena	Coryphaenidae	*P.T.*	-	38	1,820	(*33*)
Taurulus	Cottidae	*T.*	40	63	800	(*29*)
Taurulus	Cottidae	*T.*	52	63	800	"
Garra	Cyprinidae	*T.*	1	22	186	(*83*)
Garra	Cyprinidae	*T.*	2	22	235	"
Garra	Cyprinidae	*T.*	2	25	261	"
Garra	Cyprinidae	*T.*	3	29	299	"
Garra	Cyprinidae	*T.*	5	29	315	"
Garra	Cyprinidae	*T.*	6	29	326	"
Garra	Cyprinidae	*T.*	8	33	341	"
Tinca	Cyprinidae	*T.*	140	40	860	(*29*)
Tinca	Cyprinidae	*T.*	-	40	860	"
Gadidae	Gadiformes	*P.E.*	-	105	2,400	(*33*)
Tetrapturus	Istiophoridae	*P.T.*	-	48	2,220	"

Tetrapturus	Istiophoridae	*P.T.*	-	42	3,745	(*32*)
Tetrapturus	Istiophoridae	*P.T.*	-	48	4,177	(*33*)
Tetrapturus	Istiophoridae	*P.T.*	-	48	4,186	"
Tetrapturus	Istiophoridae	*P.T.*	-	45	4,291	"
Tetrapturus	Istiophoridae	*P.T.*	-	47	4,500	"
Tetrapturus	Istiophoridae	*P.T.*	-	47	4,565	"
Tetrapturus	Istiophoridae	*P.T.*	-	50	4,500	"
Symphodus	Labridae	*T.*	65	48	850	(*29*)
Isurus	Lamnidae	*P.E.*	4,620	62	1,570	(*38*)
Isurus	Lamnidae	*P.E.*	4,710	63	1,500	"
Isurus	Lamnidae	*P.E.*	5,010	67	1,750	"
Isurus	Lamnidae	*P.E.*	6,770	71	1,730	"
Isurus	Lamnidae	*P.E.*	6,950	69	1,970	"
Isurus	Lamnidae	*P.E.*	7,320	64	1,740	"
Carcharodon	Lamnidae	*P.E.*	100,000	102	3,271	(*31*)
Isurus	Lamnidae	*P.E.*	100,000	96	3,987	"
Lepisosteus	Lepisosteidae	*T.*	600	37	872	(*84*)
Lepisosteus	Lepisosteidae	*T.*	520	38	825	"
Lepisosteus	Lepisosteidae	*T.*	400	38	825	"
Lepisosteus	Lepisosteidae	*T.*	350	38	809	"
Lepisosteus	Lepisosteidae	*T.*	285	38	706	"
Lepisosteus	Lepisosteidae	*T.*	61	36	537	"
Lepisosteus	Lepisosteidae	*T.*	700	37	887	"
Lepisosteus	Lepisosteidae	*T.*	480	37	809	"
Lepisosteus	Lepisosteidae	*T.*	340	37	724	"
Lepisosteus	Lepisosteidae	*T.*	290	37	687	"
Lepisosteus	Lepisosteidae	*T.*	33	32	428	"

Lepisosteus	Lepisosteidae	*T.*	720	38	809	"
Lepisosteus	Lepisosteidae	*T.*	450	36	825	"
Lepisosteus	Lepisosteidae	*T.*	35	30	458	"
Lepisosteus	Lepisosteidae	*T.*	26	30	428	"
Lophius	Lophiidae	*T.*	1,550	91	1,100	(*29*)
Onos	Lotidae	*T.*	20	38	450	"
Onos	Lotidae	*T.*	80	50	550	"
Notothenia	Nototheniidae	*T.*	1	43	480	(*85*)
Notothenia	Nototheniidae	*T.*	3	42	480	"
Notothenia	Nototheniidae	*T.*	2	42	480	"
Notothenia	Nototheniidae	*T.*	300	67	1,070	"
Notothenia	Nototheniidae	*T.*	268	67	1,070	"
Notothenia	Nototheniidae	*T.*	280	71	1,070	"
Pleuronectes	Pleuronectidae	*T.*	86	50	750	(*29*)
Salmo	Salmonidae	*T.*	175	48	700	"
Scomber	Scombridae	*P.T.*	168	27	500	(*33*)
Katsuwonus	Scombridae	*P.T.*	965	31	1,520	"
Katsuwonus	Scombridae	*P.T.*	983	26	1,160	"
Katsuwonus	Scombridae	*P.T.*	1,056	29	1,060	"
Katsuwonus	Scombridae	*P.T.*	1,326	31	1,420	"
Katsuwonus	Scombridae	*P.T.*	2,172	29	1,420	"
Katsuwonus	Scombridae	*P.T.*	2,546	30	1,560	"
Katsuwonus	Scombridae	*P.T.*	2,758	28	1,660	"
Katsuwonus	Scombridae	*P.T.*	3,764	35	2,000	"
Katsuwonus	Scombridae	*P.T.*	5,425	35	1,880	"
Katsuwonus	Scombridae	*P.T.*	7,010	30	2,180	"
Thunnus	Scombridae	*P.T.*	1,823	29	1,220	"

Thunnus	Scombridae	*P.T.*	4,056	33	1,480	"
Thunnus	Scombridae	*P.T.*	5,035	37	1,820	"
Thunnus	Scombridae	*P.T.*	6,497	35	2,020	"
Thunnus	Scombridae	*P.T.*	9,997	36	2,400	"
Thunnus	Scombridae	*P.T.*	10,537	37	2,240	"
Thunnus	Scombridae	*P.T.*	65,421	40	3,220	"
Thunnus	Scombridae	*P.T.*	272,400	48	8,000	"
Acanthocybium	Scombridae	*P.T.*	107,000	37	1,400	"
Katsuwonus	Scombridae	*P.T.*	-	29	4,049	(*32*)
Thunnus	Scombridae	*P.T.*	-	30	3,879	"
Acanthocybium	Scombridae	*P.T.*	-	34	3,369	"
Acanthocybium	Scombridae	*P.T.*	-	37	4,073	"
Acanthocybium	Scombridae	*P.T.*	-	36	4,201	"
Acanthocybium	Scombridae	*P.T.*	-	35	4,107	"
Sarda	Scombridae	*P.T.*	-	31	3,188	"
Sarda	Scombridae	*P.T.*	-	29	3,228	"
Sarda	Scombridae	*P.T.*	-	32	3,784	"
Sarda	Scombridae	*P.T.*	-	32	3,784	"
Sarda	Scombridae	*P.T.*	-	30	3,791	"
Sarda	Scombridae	*P.T.*	-	31	4,009	"
Scomber	Scombridae	*P.T.*	-	28	1,843	"
Scomber	Scombridae	*P.T.*	-	27	1,768	"
Scomber	Scombridae	*P.T.*	-	28	1,798	"
Scomber	Scombridae	*P.T.*	-	28	2,005	"
Scomber	Scombridae	*P.T.*	-	28	1,985	"
Scomber	Scombridae	*P.T.*	-	28	2,090	"
Scomber	Scombridae	*P.T.*	-	29	2,094	"

Scomber	Scombridae	*P.T.*	-	27	2,178	"
Katsuwonus	Scombridae	*P.T.*	957	28	1,600	(*35*)
Katsuwonus	Scombridae	*P.T.*	1,667	31	2,200	"
Katsuwonus	Scombridae	*P.T.*	2,757	30	2,200	"
Katsuwonus	Scombridae	*P.T.*	6,351	33	2,600	"
Thunnus	Scombridae	*P.T.*	4,056	35	2,000	"
Thunnus	Scombridae	*P.T.*	14,541	37	2,900	"
Thunnus	Scombridae	*P.T.*	5,221	35	2,200	"
Thunnus	Scombridae	*P.T.*	6,129	36	2,400	"
Thunnus	Scombridae	*P.T.*	22,700	41	3,700	"
Thunnus	Scombridae	*P.T.*	24,516	41	3,800	"
Thunnus	Scombridae	*P.T.*	32,688	41	3,900	"
Thunnus	Scombridae	*P.T.*	4,313	34	2,200	"
Thunnus	Scombridae	*P.T.*	10,669	38	2,600	"
Thunnus	Scombridae	*P.T.*	12,485	37	3,100	"
Thunnus	Scombridae	*P.T.*	13,393	40	3,200	"
Thunnus	Scombridae	*P.T.*	15,209	41	3,100	"
Thunnus	Scombridae	*P.T.*	19,976	43	3,300	"
Thunnus	Scombridae	*P.T.*	4,767	39	2,100	"
Thunnus	Scombridae	*P.T.*	6,365	37	2,300	"
Thunnus	Scombridae	*P.T.*	7,945	41	2,300	"
Thunnus	Scombridae	*P.T.*	9,534	40	3,000	"
Thunnus	Scombridae	*P.T.*	16,344	40	2,600	"
Thunnus	Scombridae	*P.T.*	18,387	40	4,000	"
Thunnus	Scombridae	*P.T.*	21,338	42	4,000	"
Thunnus	Scombridae	*P.T.*	33,142	41	4,300	"
Glyptothorax	Sisoridae	*T.*	2	29	276	(*82*)

Glyptothorax	Sisoridae	*T.*	3	29	283	"
Glyptothorax	Sisoridae	*T.*	3	33	285	"
Glyptothorax	Sisoridae	*T.*	6	33	294	"
Glyptothorax	Sisoridae	*T.*	8	33	311	"
Trigla	Triglidae	*T.*	18	45	350	(*29*)
Xiphias	Xiphiidae	*P.T.*	19,000	53	4,040	(*33*)
Xiphias	Xiphiidae	*P.T.*	-	58	5,172	(*32*)
Xiphias	Xiphiidae	*P.T.*	-	62	5,746	"
Xiphias	Xiphiidae	*P.T.*	-	61	5,794	"
Xiphias	Xiphiidae	*P.T.*	-	56	5,806	"
Zeus	Zeidae	*T.*	300	67	1,100	(*29*)

[a] *T.*, *P.T.*, and *P.E.* denote Teleost, Pelagic Teleost, and Pelagic Elasmobranch, respectively.

[b]We assume that the lamellar thickness is negligible compared to the interlamellar distance, and estimate the interlamellar distance *d* as a reciprocal of the number of lamellae per unit length of the gill filament.

[c] For species whose lamellar surface area is only available, we estimate the lamella length by using the average aspect ratio of lamellae for each group.

References

1. W. Kim, T. Gilet, J. W. Bush, Optimal concentrations in nectar feeding. Proceedings of the National Academy of Sciences 108, 16618-16621 (2011).

2. W. Kim, J. W. Bush, Natural drinking strategies. Journal of Fluid Mechanics 705, 7-25 (2012).

3. D. L. Bihan, Molecular diffusion, tissue microdynamics and microstructure. NMR in Biomedicine 8, 375-386 (1995).

4. J. Nilsson, M. Anne, C.-J. Dalsgaard, Stimulation of connective tissue cell growth by substance P and substance K. Nature 315, 61-63 (1985).

5. J. B. West, Respiratory physiology: the essentials. (Lippincott Williams & Wilkins, 2012).

6. D. Gunn, The Temperature and Humidity Relations of the Cockroach (Blatta Orientalis) I. Desiccation. Journal of Experimental Biology 10, 274-285 (1933).

7. E. Edney, J. Spencer, Cutaneous respiration in woodlice. Journal of Experimental Biology 32, 256-269 (1955).

8. J. B. Graham, Ecological, evolutionary, and physical factors influencing aquatic animal respiration. American Zoologist 30, 137-146 (1990).

9. P. C. Withers, Comparative animal physiology. (Saunders College Fort Worth, TX, 1992).

10. C. Ballintijn, Efficiency, mechanics and motor control of fish respiration. Respiration physiology 14, 125-141 (1972).

11. C. Ballintijn, Muscle co-ordination of the respiratory pump of the carp (Cyprinus carpio L.). Journal of Experimental Biology 50, 569-591 (1969).

12. G. M. Hughes, A comparative approach to fish respiration. Experientia 26, 113-122 (1970).

13. D. L. Kramer, The evolutionary ecology of respiratory mode in fishes: an analysis based on the costs of breathing. Environmental Biology of Fishes 9, 145-158 (1983).

14. G. F. Holeton, D. R. Jones, Water flow dynamics in the respiratory tract of the carp (Cyprinus carpio L.). Journal of Experimental Biology 63, 537-549 (1975).

15. J.S.Clegg, The control of emergence and metabolism by external osmotic pressure and the role of free glycerol in developing cysts of artemia salina. Journal of Experimental Biology 41, 879-892 (1964).

16. P. Laurent, S. Dunel, Morphology of gill epithelia in fish. American Journal of Physiology 238, R147-R159 (1980).

17. S. F. Perry, P. Laurent, in Fish ecophysiology. (Springer, 1993), pp. 231-264.

18. P. Payan, J. Girard, N. Mayer-Gostan, Branchial ion movements in teleosts: the roles of respiratory and chloride cells. Fish Physiology 10, 39-63 (1984).

19. M. Pisam, A. Caroff, A. Rambourg, Two types of chloride cells in the gill epithelium of a freshwateradapted euryhaline fish: Lebistes reticulatus; their modifications during adaptation to saltwater. American Journal of Anatomy 179, 40-50 (1987).

20. J. Mullins, D. B. Groman, D. Wadowska, Infectious salmon anaemia in salt water Atlantic salmon (Salmo salar L.) in New Brunswick, Canada. Bulletin of the European Association of Fish Pathologists 18, 110 (1998).

21. I. Dykov, J. Lom, Histopathological changes in fish gills infected with myxosporidian parasites of the genus Henneguya. Journal of Fish Biology 12, 197-202 (1978).

22. W. Chen, D. Horton, Heat and water loss from the airways and exercise-induced asthma. Respiration 34, 305-313 (1977).

23. J. Cain, S. Livingstone, R. Nolan, A. Keefe, Respiratory heat loss during work at various ambient temperatures. Respiration Physiology 79, 145-150 (1990).

24. S. A. Miller, J. P. Harley, J. Aloi, G. Erickson, Zoology. (McGraw-Hill, 2002).

25. M. Kleiber, Body size and metabolic rate. Physiological Reviews 27, 511-541 (1947).

26. K. Schmidt-Nielsen, Scaling: why is animal size so important? , (Cambridge University Press, 1984).

27. T. A. McMahon, J. T. Bonner, W. Freeman, On size and life. (Scientific American Library New York, 1983).

28. G. Hughes, 1 General Anatomy of the Gills. Fish Physiology 10, 1-72 (1984).

29. G. Hughes, The dimensions of fish gills in relation to their function. Journal of Experimental Biology 45, 177-195 (1966).

30. D. H. Evans, J. B. Claiborne, The physiology of fishes. Marine biology series (CRC, Taylor & Francis, Boca Raton, FL, ed. 3rd, 2006), pp. 601 p., 608 p. of plates.

31. S. H. Emery, A. Szczepanski, Gill dimensions in pelagic elasmobranch fishes. The Biological Bulletin 171, 441-449 (1986).

32. N. C. Wegner, C. A. Sepulveda, K. B. Bull, J. B. Graham, Gill morphometrics in relation to gas transfer and ram ventilation in higher-energy demand teleosts: Scombrids and billfishes. Journal of Morphology

271, 36-49 (2010).

33. F. M. Sacks, L. P. Svetkey, W. M. Vollmer, L. J. Appel, G. A. Bray, D. Harsha, E. Obarzanek, P. R. Conlin, E. R. Miller, D. G. Simons-Morton, Effects on blood pressure of reduced dietary sodium and the Dietary Approaches to Stop Hypertension (DASH) diet. New England Journal of Medicine 344, 3-10 (2001).

34. P. Robotham, The Dimensions of the Gills of Fwo Species of Loach, Noemacheilus Barbatulus and Cobitis Taenia. The Journal of Experimental Biology 76, 181-184 (1978).

35. B. Muir, G. Hughes, Gill dimensions for three species of tunny. Journal of Experimental Biology 51, 271-285 (1969).

36. E. D. Stevens, Gill morphometry of the red drum, Sciaenops ocellatus. Fish Physiology and Biochemistry 10, 169-176 (1992).

37. S.-I. Umezawa, H. Watanabe, On the respiration of the killifish Oryzias latipes. Journal of Experimental Biology 58, 305-325 (1973).

38. N. C. Wegner, N. C. Lai, K. B. Bull, J. B. Graham, Oxygen utilization and the branchial pressure gradient during ram ventilation of the shortfin mako, Isurus oxyrinchus: is lamnid sharktuna convergence constrained by elasmobranch gill morphology? The Journal of experimental biology 215, 22-28 (2012).

39. F. P. Incropera, Fundamentals of heat and mass transfer. (John Wiley & Sons, 2011).

40. E. L. Cussler, Diffusion: mass transfer in fluid systems. (Cambridge university press, 2009).

41. B. A. Block, E. D. Stevens, Tuna: physiology, ecology, and evolution. (Gulf Professional Publishing, 2001), vol. 19.

42. Y. Itazawa, T. Takeda, Gas exchange in the carp gills in normoxic and hypoxic conditions. Respiration Physiology 35, 263-269 (1978).

43. E. D. Stevens, Some aspects of gas exchange in tuna. Journal of

Experimental Biology 56, 809 (1972).

44. C. M. WOOD, B. McMahon, D. McDonald, Respiratory gas exchange in the resting starry flounder, Platichthys stellatus: a comparison with other teleosts. The Journal of Experimental Biology 78, 167-179 (1979).

45. G. Hughes, A comparative study of gill ventilation in marine teleosts. Journal of Experimental Biology 37, 28-45 (1960).

46. A. Palstra, J. Planas, in Book of abstracts of the International Congress on the Biology of Fish, 03-07 August 2014, Edinburgh, United Kingdom. (2014), pp. 182-182.

47. S. P. Leys, D. I. Eerkes-Medrano, Feeding in a calcareous sponge: particle uptake by pseudopodia. The Biological Bulletin 211, 157-171 (2006).

48. C. Harris, M. Despa, K. Kelly, Design and fabrication of a cross flow micro heat exchanger. Microelectromechanical Systems, Journal of 9, 502-508 (2000).

49. P. S. Dittrich, A. Manz, Lab-on-a-chip: microfluidics in drug discovery. Nature Reviews Drug Discovery 5, 210-218 (2006).

50. T. Chovn, A. Guttman, Microfabricated devices in biotechnology and biochemical processing. TRENDS in Biotechnology 20, 116-122 (2002).

51. A. Roth-Nebelsick, D. Uhl, V. Mosbrugger, H. Kerp, Evolution and function of leaf venation architecture: a review. Annals of Botany 87, 553-566 (2001).

52. K. A. McCulloh, J. S. Sperry, F. R. Adler, Water transport in plants obeys Murray's law. Nature 421, 939-942 (2003).

53. A. Fitter, An architectural approach to the comparative ecology of plant root systems. New Phytologist 106, 61-77 (1987).

54. G. Gyssels, J. Poesen, The importance of plant root characteristics in controlling concentrated flow erosion rates. Earth Surface Processes and

Landforms 28, 371-384 (2003).

55. A. Fitter, The topology and geometry of plant root systems: influence of watering rate on root system topology in Trifolium pratense. Annals of Botany 58, 91-101 (1986).

56. B. R. Masters, Fractal analysis of the vascular tree in the human retina. Annual Review of Biomedical Engineering 6, 427-452 (2004).

57. G. S. Kassab, Scaling laws of vascular trees: of form and function. American Journal of Physiology-Heart and Circulatory Physiology 290, H894-H903 (2006).

58. J. R. Less, T. C. Skalak, E. M. Sevick, R. K. Jain, Microvascular architecture in a mammary carcinoma: branching patterns and vessel dimensions. Cancer research 51, 265-273 (1991).

59. T. F. Sherman, On connecting large vessels to small. The meaning of Murray's law. The Journal of General Physiology 78, 431-453 (1981).

60. E. R. Weibel, B. Sapoval, M. Filoche, Design of peripheral airways for efficient gas exchange. Respiratory Physiology & Neurobiology 148, 3-21 (2005).

61. B. Mauroy, M. Filoche, E. Weibel, B. Sapoval, An optimal bronchial tree may be dangerous. Nature 427, 633-636 (2004).

62. K. Pump, The morphology of the finer branches of the bronchial tree of the human lung. CHEST Journal 46, 379-398 (1964).

63. K. McCulloh, J. Sperry, F. Adler, Murray's law and the hydraulic vs mechanical functioning of wood. Functional Ecology 18, 931-938 (2004).

64. C. D. Murray, The physiological principle of minimum work: I. The vascular system and the cost of blood volume. Proceedings of the National Academy of Sciences of the United States of America 12, 207 (1926).

65. C. D. Murray, The physiological principle of minimum work applied to the angle of branching of arteries. The Journal of General Physiology 9, 835-841 (1926).

66. T. A. Wilson, Design of the bronchial tree. Nature 213, 668-669 (1967).

67. B. HaefeliBleuer, E. R. Weibel, Morphometry of the human pulmonary acinus. The Anatomical Record 220, 401-414 (1988).

68. E. R. Weibel, D. M. Gomez, Architecture of the Human Lung Use of quantitative methods establishes fundamental relations between size and number of lung structures. Science 137, 577-585 (1962).

69. E. R. Weibel, Morphometry of the human lung. (Springer, 1965).

70. W. H. Finlay, C. F. Lange, M. King, D. P. Speert, Lung delivery of aerosolized dextran. American Journal of Respiratory and Critical Care Medicine 161, 91-97 (2000).

71. S. Gheorghiu, S. Kjelstrup, P. Pfeifer, M.O. Coppens, Gas diffusion through the fractal landscape of the lung: How deep does oxygen enter the alveolar system? In Fractals in Biology and Medicine (Springer, 2005), pp. 31-42.

72. B. Sapoval, M. Filoche, Magic trees in mammalians respiration or when evolution selected clever physical systems. Fractals 21, (2013).

73. B. Sapoval, M. Filoche, E. Weibel, Smaller is betterbut not too small: a physical scale for the design of the mammalian pulmonary acinus. Proceedings of the National Academy of Sciences 99, 10411-10416 (2002).

74. Y. Liu, G. S. Kassab, Vascular metabolic dissipation in Murray's law. American Journal of Physiology-Heart and Circulatory Physiology 292, H1336-H1339 (2007).

75. D. R. Emerson, K. Cielicki, X. Gu, R. W. Barber, Biomimetic design of microfluidic manifolds based on a generalised Murray's law. Lab on a Chip 6, 447-454 (2006).

76. H. Williams, R. Trask, P. Weaver, I. Bond, Minimum mass vascular networks in multifunctional materials. Journal of the Royal Society Interface 5, 55-65 (2008).

77. C. L. Hansen, E. Skordalakes, J. M. Berger, S. R. Quake, A robust and scalable microfluidic metering method that allows protein crystal growth by free interface diffusion. Proceedings of the National Academy of Sciences 99, 16531-16536 (2002).

78. E. A. Schilling, A. E. Kamholz, P. Yager, Cell lysis and protein extraction in a microfluidic device with detection by a fluorogenic enzyme assay. Analytical Chemistry 74, 1798-1804 (2002).

79. S.-Y. Cheng, S. Heilman, M. Wasserman, S. Archer, M. L. Shuler, M. Wu, A hydrogel-based microfluidic device for the studies of directed cell migration. Lab on a Chip 7, 763-769 (2007).

80. G. Hughes, S. Dube, J. Munshi, Surface area of the respiratory organs of the climbing perch, Anabas testudineus (Pisces: Anabantidae). Journal of Zoology 170, 227-243 (1973).

81. F. Galis, C. Barel, Comparative functional morphology of the gills of African lacustrine Cichlidae (Pisces, Teleostei). Netherlands Journal of Zoology 30, 392-430 (1979).

82. B. Singh, A. Yadav, J. Ojha, J. D. Munshi, Gross structure and dimensions of the gills of an intestinal airbreathing fish (Lepidocephalichthys guntea). Copeia, 224-229 (1981).

83. G. L. Joseph, Respiratory surface area (gill area) of the hillstream fish Garra mullya (Sykes). Indian Journal of Fisheries 27, 172-176 (1980).

84. J. C. Landolt, L. G. Hill, Observations of the gross structure and dimensions of the gills of three species of gars (Lepisosteidae). Copeia, 470-475 (1975).

85. J. E. M. Westermann, D. L. Barber, L. G. Malo, Observations on gills of pelagic and demersal Juvenile northenia rossh. British Antarctic Survey Bulletin 65, 81-89(1984).

Abstract (in Korean)

초 록

자연에서 발견할 수 있는 다양한 생체기관은 개체의 생존에 도움을 주는 방향으로 오랜 시간 동안 진화하였다. 그렇기 때문에 우리는 막연하게 생체기관의 구조가 본연의 기능적 효율을 최대로 하는 최적구조를 가지고 있다고 생각한다. 그러나 생체기관은 우리가 쉽게 파악하지 못 할 만큼 충분히 복잡하여 생체기관이 무엇을 어떻게 최적화 하였는지에 대해서 명확히 정의하는 것은 어려운 문제이다. 우리는 이번 연구에서 기존에는 알려지지 않았던 물고기의 아가미 구조와 인간의 폐 도관 구조의 최적화 방식에 대해 가설을 제시하였고, 이를 유체역학적 해석, 생리학적 데이터 분석, 수학적 모델링, 마이크로 스케일에서의 유체 실험 등을 통해 검증하였다.

물고기 아가미 연구에서, 아가미 필라멘트 위에 나란하게 배열되어 넓은 기체 교환 표면적을 제공하는 라멜라 배열이 물고기의 종과 크기에 관계없이 일정한 간격을 유지한다는

사실을 발견하였다. 우리는 라멜라 간격의 크기에 따라 산소 전달량이 어떻게 변하는지 유체역학적으로 해석하였고, 이를 아가미 구조를 모사한 마이크로 칩을 제작하여 검증하였다. 이를 통해 우리는 실제 물고기들의 라멜라 배열 간격이 아가미 내부 압력과 라멜라 길이에 따라 산소 전달량을 최대로 하도록 정해진다는 것을 밝혀내었다.

인간의 폐는 줄기 도관이 가지 도관으로 두 개씩 연속적으로 분지한 나무 구조를 가지고 있다. 기도와 가까운 쪽에 위치한 대류 도관의 경우 직경 감소 비율이 점성 에너지 소산을 최소화 하기 위한 최적 구조를 가지고 있다고 밝혀져 있다. 그러나 대류도관 아래쪽에 위치한 확산 도관의 직경 감소 비율이 정해지는 원리는 밝혀지지 않았었다. 우리는 확산 도관의 직경 감소 비율은 확산 도관에서의 신진 대사 에너지 소비를 최소화 하면서 산소 흡수를 원활히 하는 구조를 가지고 있을 것이라 가정하였다. 이를 유체역학적 해석과 해석 과정 중 나타나는 비정상 편미분 방정식을 변수 분리 및 스텀 리우빌 이론을 응용하여 수학적으로 모델링 하였다. 우리의 수학적 모델링은 실제 폐의 확산 도관 직경 감소 비율이 작동

에너지 효율을 극대화 하기에 최적의 비율이라는 것을 보여준다.

주요어: 생체모방공학, 생체유체역학, 아가미, 폐, 호흡

학 번: 2008 - 20743